

Disentangling the Signatures of Blended-Light Atmospheres in L/T Transition Brown Dwarfs

AFRA ASHRAF,^{1,2} DANIELLA C. BARDALEZ GAGLIUFFI,² ELENA MANJAVACAS,³
JOHANNA M. VOS,² CLAIRE MECHMANN,⁴ AND JACQUELINE K. FAHERTY²

¹*Department of Physics & Astronomy, Barnard College
3009 Broadway, New York, NY 10027, USA*

²*Department of Astrophysics, American Museum of Natural History
200 Central Park West, New York, NY 10024, USA*

³*AURA for the European Space Agency (ESA), ESA Office, Space Telescope Science Institute, 3700
San Martin Drive, Baltimore, MD, 21218 USA*

⁴*Department of Physics & Astronomy, Lehman College, City University of New York
250 Bedford Park Blvd W, The Bronx, NY 10468, USA*

Submitted to ApJ

ABSTRACT

We present a technique to identify spectrophotometrically variable L7–T3 brown dwarfs with single-epoch, low-resolution, near-infrared SpeX spectra. We calculated spectral indices on known variable brown dwarfs and used them to select 11 index-index parameter spaces where known variables can be distinguished from the rest of the general population of brown dwarfs. We find 62 candidate variables, 12 of which show significant variability amplitude in independent photometric monitoring surveys. This technique constitutes the first formal method to identify a time-dependent effect such as variability from peculiarities in their integrated light spectra. This technique will be a useful tool to prioritize targets for future photometric and spectroscopic monitoring in the era of *JWST* and 30 m-class telescopes.

Keywords: Brown dwarfs (185), L dwarfs (894), T dwarfs (1679), Atmospheric variability (2119), Astronomical techniques (1684), Near infrared astronomy (1093), Spectroscopy (1558)

1. INTRODUCTION

Substellar variability is a time-dependent phenomenon caused by an inhomogeneous atmosphere over the course of an object’s rotation period, and it is characterized by a change in flux over time. Photometric variability is dominated by magnetic activity in M dwarfs and early-L dwarfs (Hawley 1993) and by inhomogeneous cloud coverage in cooler brown dwarfs (Gelino et al. 2002). The cool temperatures of L and T-type brown dwarf atmospheres permit the condensation of different species, resulting in patchy layers of large-scale cloud and haze structures (Ackerman & Marley 2001). Different elements and compounds reach their condensation equilibrium at varying temperatures and pressures, such that clouds can form at different altitudes in the atmosphere. Silicate and iron condensates begin to form in the atmospheres of L-dwarfs below 2400 K (Lodders & Fegley 2006). Towards the end of the L sequence, silicate and iron clouds sink beneath the photosphere in what is known as “rain out” (Knapp et al. 2004). By the time an object has cooled down to T dwarf temperatures, their clouds have sunken below the photospheres. The sudden increase in brightness in the J -band for late-L/early-T brown dwarfs (called the “J-band bump”) has been interpreted as evidence for this process (Burgasser et al. 2002a; Dahn et al. 2002; Tinney et al. 2003; Vrba et al. 2004). An alternative explanation for photometric variability is a cloudless model, where variations arise due to a convective atmosphere dominated by CO/CH₄ radiative convection as shown in Tremblin et al. (2015, 2016, 2017, 2019, 2020).

The L/T transition is a critical phase in the evolution of brown dwarfs which happens over a relatively short range of effective temperatures ($1150 \text{ K} \lesssim T_{eff} \lesssim 1350 \text{ K}$; Vos et al. 2019a; Filippazzo et al. 2015) and is characterized by the appearance of methane in near-infrared (NIR) spectra and a shift towards blue in $J - H$ and $H - K$ colors. Strong NIR variability is most common within this spectral type range, with a 24% variability occurrence (amplitudes $> 2\%$) compared to only 3.2% outside of the L/T transition (Radigan 2014). Since variability is thought to be more prevalent in this spectral type region, we have the best chance of identifying suitable targets amenable for further study.

However, variability studies are extremely resource intensive. Reliable light curves require precision photometric monitoring over the course of several hours for each target, covering a significant portion of an object’s rotation period. For example, in their photometric variability survey, Radigan et al. (2014) obtained 62 light curves of L4–T9 dwarfs with 2 – 3 m aperture ground-based telescopes spanning roughly 2-5 hours per target. Accounting for telescope slewing, target acquisition and data read out, these observations amounted to almost 250 hours of on-sky time, resulting in variability detection in 16% of their targets. In their space-based variability survey, Metchev et al. (2015) targeted 44 L3–T8 brown dwarfs and identified 19 objects, i.e. $61^{+17}_{-20}\%$ of L dwarfs and $31^{+35}_{-17}\%$ of T dwarfs, as having photometric variability with an amplitude of 0.2 – 4.6% using the *Spitzer Space Telescope*. Likewise, Buenzli et al. (2014) found 6 variable brown dwarfs in a sample of 22 observed with the *Hubble Space*

Telescope. These surveys are crucial to understand the occurrence of variability and to study the time-dependent atmospheric dynamics and vertical structure of brown dwarf atmospheres at a population level, yet such surveys cannot pre-select candidates based on their likelihood to show variability because currently there is no systematic way to prioritize candidates for variability studies.

Spectral binaries may hold a clue for such a technique. Spectral binaries are systems of two brown dwarfs of different spectral types with a combined peculiar unresolved, low-resolution, NIR spectrum (Cruz et al. 2004; Burgasser 2007a; Burgasser et al. 2010; Bardalez Gagliuffi et al. 2014). Spectral binary candidates are identified using spectral indices and binary template fitting, and later confirmed through high resolution imaging, radial velocity or astrometric variability (e.g., Bardalez Gagliuffi et al. 2015; Burgasser et al. 2016; Sahlmann et al. 2020). However, a handful of spectral binary candidates have not shown signs of binarity in high resolution follow-up and instead are known to show photometric variability. The young early-T dwarfs 2MASS J21392676+0220226 (hereafter J2139+0220, Burgasser et al. 2006a) and 2MASS J13243553+6358281 (hereafter J1324+6358,Looper et al. 2007), were originally suggested to be spectral binary candidates (Burgasser et al. 2010) of L4 and T5 components, but are actually single, photometrically variable brown dwarfs (Radigan et al. 2012; Metchev et al. 2015). This suggests that the spectral binary technique may also be inadvertently sensitive to the type of inhomogeneous atmospheres that drive variability.

Khandrika et al. (2013) searched for photometric variability in *J* and *K*-bands using the Gemini infrared camera on the 3-meter Shane Telescope at Lick Observatory for 15 L and T-type brown dwarfs, including 7 spectral binary candidates. They found variability in 4 objects, two of which were spectral binary candidates at the time, 2MASS J2139+0220 and SDSS J141624.08+134826.7A (hereafter J1416+1348A, Scholz 2010). In their spectroscopic variability program with *Hubble Space Telescope's* Wide Field Camera 3, Manjavacas et al. (2019) used the spectral binary technique to identify peculiar sources and multiple systems. However, they discovered that five of the eight spectral binary candidates they found had been previously identified in the literature as photometrically variable. Sources like 2MASS J2139+0220, 2MASS J1324+6358, and SDSS J1416+1348A, while originally selected as spectral binary candidates, present no compelling signs of binarity and instead show significant variability amplitudes. These motivating examples suggest that the spectral signatures caused by two separate sources at different temperatures on an unresolved spectrum are similar to those of a single object with multiple cloudy, patchy layers at different temperatures. The peculiarities in the spectra selected by index-based spectral binary techniques may instead be occasionally caused by cloud-driven variability.

Cloud-driven brown dwarf variability is also correlated with age. Young brown dwarfs have redder near-infrared and mid-infrared colors in comparison to field ob-

jects of the same spectral type. This is likely due to their low surface gravity and extended radii from their ongoing contraction, leading to slower sedimentation efficiency of scattering particles like dust grains in their atmospheres (Faherty et al. 2016). In the *Weather on Other Worlds* survey by Metchev et al. (2015), they found an association with 92% confidence between low surface gravity and high-amplitude variability among L3 - L5.5 dwarfs. Vos et al. (2019b) calculated a variability occurrence rate in a sample of L0-L8.5 young, low-gravity objects using the New Technology Telescope (NTT) and the United Kingdom InfraRed Telescope (UKIRT) of $30_{-8}^{+16}\%$ which they compared to the results of Radigan et al. (2014) where the field dwarfs have a variability occurrence rate of $11_{-4}^{+13}\%$. These results suggest that variability occurs more frequently and has a higher amplitude in young brown dwarfs. Marley et al. (2012) suggests that this correlation could be caused by high altitude clouds in low-gravity atmospheres, increasing the contrast between different cloud layers. In a recent variability survey, Vos et al. (2022) indeed finds that the maximum variability amplitudes observed for low-gravity L dwarfs are higher compared to field objects.

Variability studies in brown dwarfs are precursors to future studies of exoplanet climates. Brown dwarfs are characterized by physical properties that are very similar in nature to extrasolar planets, in particular directly-imaged exoplanets or young giant planets. L and T-type dwarfs overlap in temperature range ($500 \text{ K} \lesssim T_{eff} \lesssim 2300 \text{ K}$; Filippazzo et al. 2015) with young giant exoplanets ($1300 \text{ K} \lesssim T_{eff} \lesssim 3000 \text{ K}$; Madhusudhan et al. 2014), a parallel reflected in their atmospheric spectra. However, brown dwarfs are much easier to image than exoplanets since they are typically unobstructed by a host star, making atmospheric studies more accessible. Apai et al. (2016) and Biller et al. (2021) probed the giant exoplanets in the HR8799 system for variability using VLT/SPHERE, but neither could achieve high enough sensitivity to confidently detect variability. This highlights the importance of studying isolated planetary-mass objects as analogs to exoplanets in orbit around a bright host star.

The emergence of next-generation telescopes, such as the *James Webb Space Telescope (JWST)*, will permit detailed characterization of exoplanets (Carter et al. 2021), and the techniques used to study brown dwarf atmospheres will be important predecessors to surface mapping and characterizing exoplanet atmospheres. We can analyze light curves to obtain variability amplitudes and rotation periods. By using stellar and substellar light curves, we can map the surface inhomogeneities of stars with topological light curve inversion and modeling (Apai et al. 2017; Luger et al. 2019), albeit with degeneracies. The same techniques will be applied to exoplanets with time-resolved high-contrast imaging. Our technique potentially offers an opportunity to probe the vertical structure of the atmosphere to complement the surface information provided by light curves and compare to 3D global circulation models (Showman et al. 2019; Tan & Showman 2021a).

In this paper we present a new technique to identify high likelihood variability candidates among L7–T3 dwarfs based on spectral indices of single-epoch, low res-

olution, NIR spectra. In Section 2, we discuss the characteristics of our sample. In Section 3, we use our technique to identify variability candidates for follow-up photometric monitoring. In Section 4 we discuss the stability of SpeX as an instrument, calculate our variability fractions, and examine the possible surface features that could cause different variability amplitudes. Finally in Section 5 we present our conclusions.

2. SPEX SPECTRAL SAMPLE

Our spectral sample was retrieved from the SpeX Prism Library (SPL; [Burgasser 2014](#)) and is composed of 325 spectra from 270 unique objects within the L7–T3 dwarf spectral type range ($1150\text{ K} \lesssim T_{eff} \lesssim 1350\text{ K}$). The SPL contains over 2000 NIR spectra of ultracool and brown dwarfs collaboratively collected since the year 2000 with SpeX, a spectrograph mounted on the 3-m NASA Infrared Telescope Facility in Mauna Kea, HI ([Vacca et al. 2003](#); [Rayner et al. 2003](#)). We used spectra in the SPL acquired with the prism-dispersed mode of SpeX, which samples wavelengths between 0.75 and $2.5\mu\text{m}$ at a dispersion of $20\text{--}30\text{ \AA pixel}^{-1}$. The spectra contained in the SPL have been homogeneously obtained with the same observing strategy (see e.g., [Bardalez Gagliuffi et al. 2014, 2019](#); [Burgasser et al. 2010](#) for technical details on acquisition, integration, calibration, and reduction of SpeX spectra).

Since we are interested in identifying differences between variable and non-variable objects across spectral features, such as a peculiar slope or depth of absorption lines and bands, we restrict our sample to spectra acquired in a single epoch. This means that we are not using spectra intended for spectroscopic variability, which involves a series of short-exposure spectra in a large field of view including reference stars to evaluate the change of spectral features over time. Depending on how well the slit was aligned with the parallactic angle to avoid slit losses, and the duration of integration at the time of observations, the flux of an individual spectrum may fluctuate between 1-2% of the total flux on separate epochs because of atmospheric turbulence (M. Connelley, priv. comm.).

We use the SpeX spectral classifications from the SPL, which follow the [Kirkpatrick et al. \(2010\)](#) standards and method that only use the J -band for spectral classification for L-dwarfs and the [Burgasser et al. \(2006a\)](#) near-infrared spectral type standards for T-dwarfs. We excluded subdwarfs and sources in star-forming regions as we wanted to focus on differences in spectra caused by cloud-driven variability, not by other factors like reddening or low metallicity that would result in unusual spectra. The spectra were calibrated to absolute flux densities using their 2MASS J -band magnitudes and the empirical relations of [Filippazzo et al. \(2015\)](#), with the flux calibration function within the *SPLAT* package.

Given the correlation between variability and age, we identified young objects within our sample following the literature. Of the 325 spectra examined, there are a total of 51 young spectra from 49 young objects, of which 4 are confirmed variables from

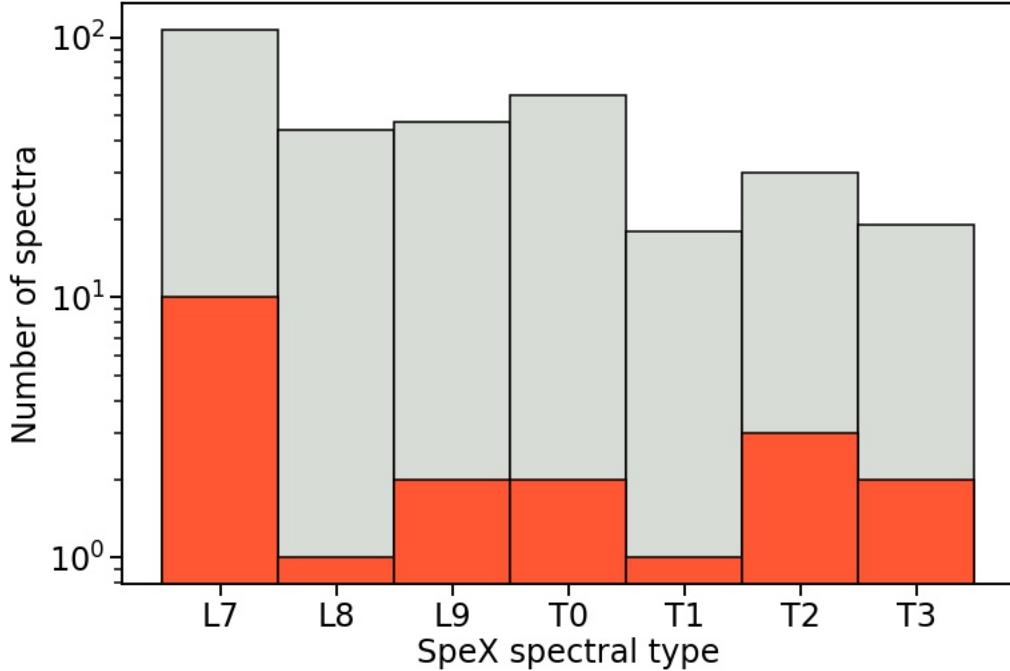


Figure 1. *Spectral type distribution of our sample with benchmark variables in red.*

photometric monitoring. We consider objects as “young” according to the literature, given spectral features and kinematics significantly different from those in field objects, which are evident up to roughly 150 Myr old (e.g., the age of the AB Doradus moving group, [Faherty et al. 2016](#)). Objects with high space velocities relative to the Sun tend to have older ages, as they have had a long time to accumulate energy kicks from gravitational interactions with other stars on their orbit around the galactic center. Gravity estimates can be obtained from spectral features in low resolution spectra ([Allers & Liu 2013](#)) and age estimates by kinematic association to a young moving group, which like the Pleiades, AB Doradus, or the Hyades, are coeval, gravitationally-bound groups of stars. Additionally, we identify 13 spectra from 8 confirmed spectral binaries. The spectral type distribution of our final sample is shown in Figure 1, highlighting variable sources. Since the SPL is a general repository of spectra observed for a variety of science cases, we do not claim our selected sample to be unbiased or complete.

3. IDENTIFICATION OF CANDIDATE VARIABLES

3.1. Benchmarks

From our sample of L/T transition objects, we select as “benchmarks” 21 spectra from 15 objects that have confirmed light curve amplitudes $> 1\%$ in J , $[3.6]$, or $[4.5]$ bands from previous time-resolved, photometric monitoring across several variability studies varying in sensitivity and/or wavelength coverage (see Table 1 and [Vos](#)

et al. 2020 for a summary of sources with measured variability). Ground-based near-infrared surveys (e.g. Radigan et al. 2014; Vos et al. 2019b) are generally sensitive to variations greater than 1 – 2%, and can only observe each target as long as it is visible. Variability studies that use the WFC3 instrument on the Hubble Space Telescope (e.g. Apai et al. 2013; Buenzli et al. 2014) reach precisions of 0.01 – 0.02%, but have generally been limited in observing duration. Finally, variability studies using the Spitzer Space Telescope (e.g. Metchev et al. 2015; Vos et al. 2022) achieve both sub-percent precision and relatively long monitoring duration (~ 20 hr). Variability monitoring with the Spitzer Space Telescope is likely the most sensitive to date for detecting variability in L and T brown dwarfs, yielding lower mid-IR amplitudes when compared to near-IR amplitudes. Our strict benchmark selection process discounted 8 objects from the literature with either upper limits in variability amplitudes (i.e., no variability or variability below the sensitivity limit) or previous identification as spectral binary candidates from the benchmark list that were later recovered as variability candidates: SDSS J0758+3247, SDSS J0858+3256, 2MASS J1119-1137, SDSS J1219+3128, SDSS J1254-0122, SDSS J1516+3053, 2MASS J1632+1904, 2MASS J2224-0158. This was also the case for Luhman 16A, which we decided to exclude from the benchmarks list due to contrasting reports of variability in the NIR and MIR.

The variability amplitudes in the NIR for our benchmarks range from 1.2% to 26% for 2MASS J21392676+0220226 (Radigan et al. 2012) in J -band, including Luhman 16B (11% in WFC3-IR at 1.1-1.66 μm Buenzli et al. 2015b). Three of our benchmarks only have variability measurements in *Spitzer* [3.6] or [4.5] bands with amplitudes between 1-3%. While 2MASS J20025073-0521524 and 2MASSW J0310599+164816 do not have a measured rotation period, the rest of our benchmarks have periods between 2-19 h. While the planetary-mass, L7 dwarf PSO 318.5-22 (Liu et al. 2013) qualifies as a benchmark given our criteria, we did not have a SpeX spectrum of this source in the SPL. Sources that had been previously selected as spectral binary candidates and for which no high-resolution imaging is available were excluded. This cut affected SDSS J075840.33+324723.4 and SDSS J151643.01+305344.4, both of which were identified as variability candidates with our technique. We excluded the blended light spectrum of Luhman 16AB from our benchmark list, but kept the individual spectrum of the spatially resolved B component. The B component is a T0 dwarf with a large variability amplitude of $\sim 11\%$ (Gillon et al. 2013), which gets diminished in the combined-light spectrum. We also excluded the unresolved spectrum of 2MASSI J0423485–041403 (hereafter 2MASS J0423–0414), because even though it is a known variable (0.8% J -band amplitude, Radigan et al. 2014), it is also an astrometric binary system (Dupuy & Liu 2012).

3.2. Selection regions in index-index spaces

Table 1. Confirmed variability sources used as benchmarks in our study.

Source	Spectral type			Reference (Optical SpT; Youth; Variability)
	Optical	NIR SpeX	Young?	
WISEP J004701.06+680352.1	L7pec	L7	Y	7; 8; 12, 20
SDSSp J010752.33+004156.1	L8	L7	Y	9; ... ; 15
SIMP J013656.57+093347.3	...	T2	Y	... ; 3; 16
2MASSW J0310599+164816	L8	T0	N	10; ... ; 1
2MASSI J0825196+211552	L7.5	L8	N	10; ... ; 15
SDSS J104335.08+121314.1	...	L9	N	... ; ... ; 15
WISE J104915.57−531906.1B	T1	T1	N	11; ... ; 5
SDSS J105213.51+442255.7	...	T0	N	... ; ... ; 6
2MASS J11472421−2040204	...	L7	Y	... ; 18; 15
2MASS J13243553+6358281	...	T3	Y	... ; 4; 15
2MASS J16291840+0335371 (PSO J247.3273+03.5932)	...	T2	N	... ; ... ; 16
2MASS J20025073−0521524	L6	L7	N	2; ... ; 21
2MASS J21392676+0220226	...	T2	Y	... ; 23; 17
HN Peg B	...	T3	Y	... ; 14; 15
2MASS J21481628+4003593	L6	L7.0	Y	13; 22; 15, 19

References—(1) Buenzli et al. (2015b); (2) Cruz et al. (2007); (3) Gagné et al. (2017a); (4) Gagné et al. (2018a); (5) Gillon et al. (2013); (6) Girardin et al. (2013); (7) Gizis et al. (2012); (8) Gizis et al. (2015); (9) Hawley et al. (2002); (10) Kirkpatrick et al. (2000); (11) Kniazev et al. (2013); (12) Lew et al. (2016), (13) Looper et al. (2008); (14) Luhman et al. (2007); (16) Metchev et al. (2015); (15) Radigan (2014); (17) Radigan et al. (2014); (18) Schneider et al. (2016b); (19) Vos et al. (2017); (20) Vos et al. (2018); (21) Vos et al. (2019b); (22) Vos et al. (2020); (23) Zhang et al. (2021)

In order to identify signatures of variability from single-epoch spectra, we modified the spectral indices techniques from Bardalez Gagliuffi et al. (2014) and Burgasser et al. (2010), originally designed to identify spectral binary candidates of late-M and L dwarf primaries with a T-dwarf companion. The 13 indices examined are: H_2O - J , CH_4 - J , J -curve, CH_4 - H , H_2O - H , K/J , J -slope, H_2O - Y , H -bump, H -dip, H_2O - K , CH_4 - K , and K -slope, which are specified in Bardalez Gagliuffi et al. (2014) and span the NIR range across J , H , and K bands. The wavelength ranges that correspond to each spectral index are shown in Figure 2 and Table 2. We calculated spectral indices by integrating the flux column enclosed by these wavelength regions and finding the ratio between them.

We measured these indices on our entire spectral sample and compared them against each other to identify regions of variability based on visual inspection. We visually examined 78 index-index plots using 21 spectra of 15 sources with confirmed variability from photometric monitoring as our benchmarks (see Section 3.1) to define variability regions in each index-index plot. From these index-index plots, we selected 11 parameter spaces where the benchmark variables were differentiated from the general spectral sample (Figure 3). We defined polygonal regions within these plots which conservatively contain all the benchmark variables. The limits for each region in the index-index plots are shown in Table 3 and illustrated in Figure 3.

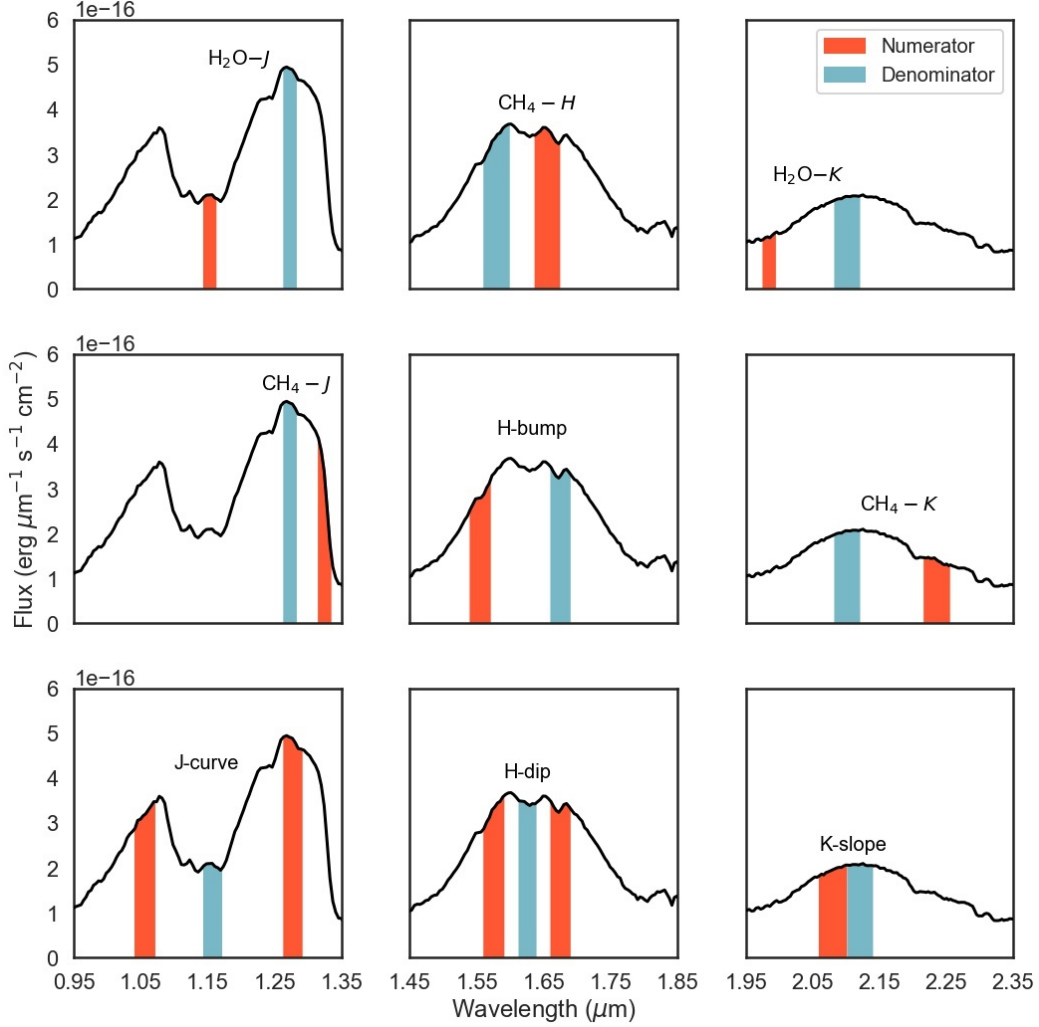


Figure 2. Locations of wavelength regions used to calculate spectral indices superimposed on a sample brown dwarf spectrum. Spectral indices are obtained by integrating the flux column defined by these wavelength regions and finding the ratio between them. For cases where 3 flux columns are used, an average of two flux columns of the same color are used as either numerator or denominator.

We defined variability candidacy based on the number of times a spectrum was found within our variability regions. Figure 4 shows the frequency with which spectra were identified in a given number of index-index plots. All of our benchmark sources, which are confirmed variables, are found in all 11 index-index plots by design, except for one of the two spectra of the L5.5 dwarf 2MASS J20025073-0521524 (hereafter 2MASS J2002-0521, Vos et al. 2019b). For this reason, we define weak candidates as sources which fall in 10 regions and strong candidates those which are found in all 11 regions in our index-index plots. This criterion results in 51 strong and 11 weak candidate variable sources amenable for future photometric monitoring.

3.3. Notable Sources

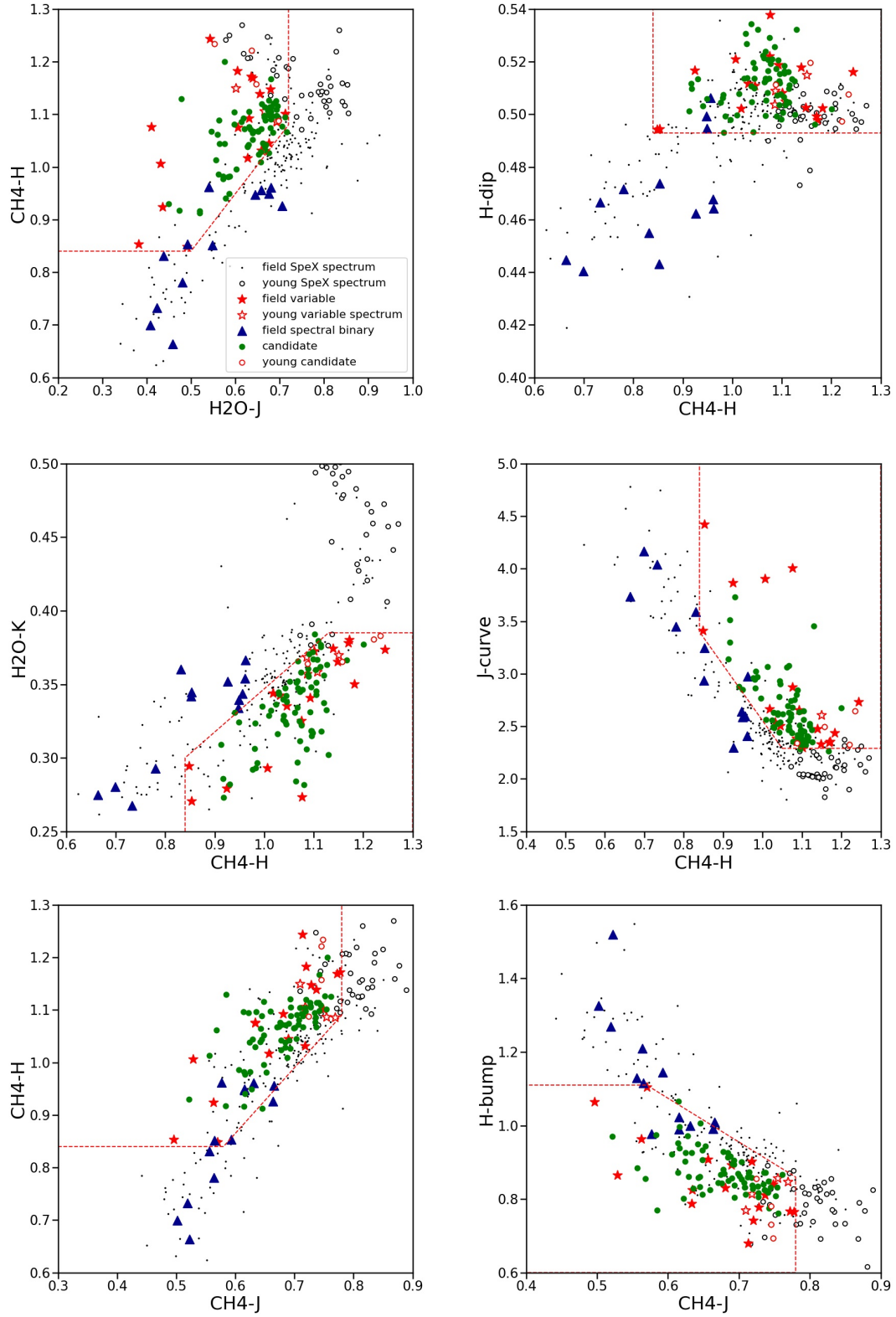


Figure 3. The 11 index-index plots used to identify variability candidates. The red stars indicate our benchmark variables. The blue triangles indicate confirmed spectral binaries. The open stars and open circles indicate youth, while everything that is filled in is a field object.

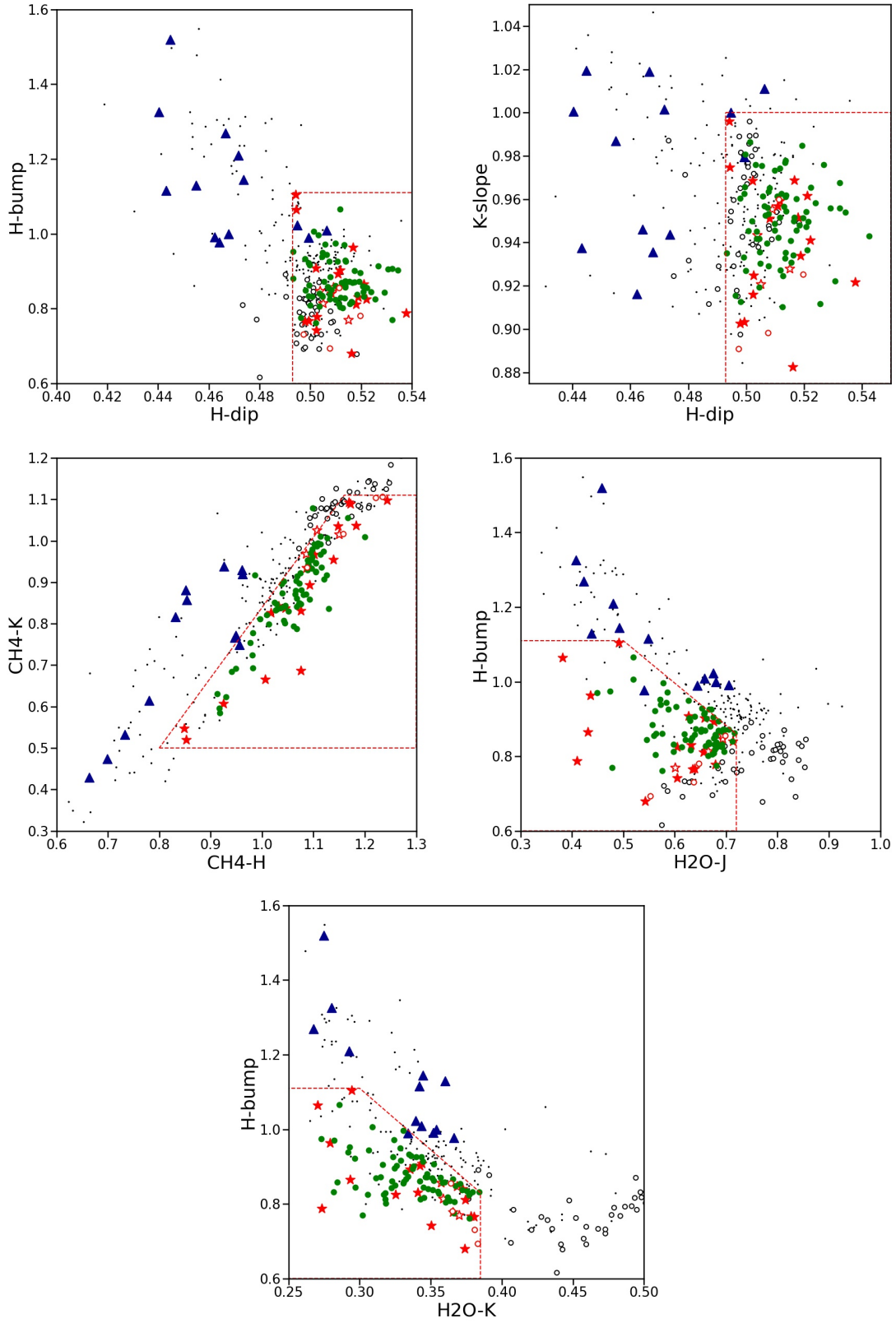


Figure 3. continued

Table 2. Wavelength Ranges of Spectral Indices

Spectral Index	Numerator Range (μm)	Denominator Range (μm)	Feature	Reference
H ₂ O- <i>J</i>	1.14-1.165	1.26-1.285	1.15 μm H ₂ O	1
CH ₄ - <i>J</i>	1.315-1.335	1.26-1.286	1.32 μm CH ₄	1
<i>J</i> -curve	1.04-1.07 + 1.26-1.29	1.14-1.17	Curvature across <i>J</i> -band	4
CH ₄ - <i>H</i>	1.635-1.675	1.56-1.60	1.65 μm CH ₄	1
<i>H</i> -bump	1.54-1.57	1.66-1.69	Slope across <i>H</i> -band peak	4
<i>H</i> -dip	1.61-1.64	1.56-1.59 + 1.66-1.69	1.63 μm FeH/CH ₄	2
H ₂ O- <i>K</i>	1.975-1.995	2.08-2.10	1.90 μm H ₂ O	1
CH ₄ - <i>K</i>	2.215-2.255	2.08-2.12	2.20 μm CH ₄	1
<i>K</i> -slope	2.06-2.10	2.10-2.14	<i>K</i> -band shape/CIA H ₂	3

NOTE—Numerical values of the wavelength regions of the spectral indices shown in Figure 2. For the indices where the range has a plus sign, the range is the average of the two wavelength ranges listed.

References—(1) Burgasser et al. (2006a); (2) Burgasser et al. (2010); (3) Burgasser et al. (2002b); (4) Bardalez Gagliuffi et al. (2014).

Table 3. Region limits for each index-index correlation plot.

x-axis	y-axis	coordinates	x-range	y-range
H2O- <i>J</i>	CH4- <i>H</i>	[[0.2,0.84],[0.5,0.84],[0.72,1.08],[0.72,1.3],[0.2,1.3],[0.2,0.84]]	[0.2,1]	[0.6,1.3]
H2O- <i>J</i>	<i>H</i> -bump	[[0.2,1.11],[0.5,1.11],[0.72,0.86],[0.72,0.6],[0.2,0.6],[0.2,1.11]]	[0.3,1]	[0.6,1.6]
CH4- <i>J</i>	CH4- <i>H</i>	[[0.3,0.84],[0.58,0.84],[0.78,1.09],[0.78,1.3],[0.3,1.3],[0.3,0.84]]	[0.3,0.9]	[0.6,1.3]
CH4- <i>J</i>	<i>H</i> -bump	[[0.3,1.11],[0.57,1.11],[0.78,0.86],[0.78,0.6],[0.3,0.6],[0.3,1.11]]	[0.4,0.9]	[0.6,1.6]
CH4- <i>H</i>	H2O- <i>K</i>	[[0.84,0.2],[0.84,0.3],[1.13,0.385],[1.3,0.385],[1.3,0.2],[0.84,0.2]]	[0.6,1.3]	[0.25,0.5]
CH4- <i>H</i>	CH4- <i>K</i>	[[0.8,0.5],[1.3,0.5],[1.3,1.11],[1.16,1.11],[0.8,0.5]]	[0.6,1.3]	[0.3,1.2]
CH4- <i>H</i>	<i>H</i> -dip	[[0.84,0.493],[1.3,0.493],[1.3,0.54],[0.84,0.54],[0.84,0.493]]	[0.6,1.3]	[0.4,0.54]
CH4- <i>H</i>	<i>J</i> -curve	[[1.05,2.29],[1.3,2.29],[1.3,5.5],[0.84,5.5],[0.84,3.4],[1.05,2.29]]	[0.4,1.3]	[1.5,5.0]
H2O- <i>K</i>	<i>H</i> -bump	[[0.2,1.11],[0.3,1.11],[0.385,0.83],[0.385,0.6],[0.2,0.6],[0.2,1.11]]	[0.25,0.5]	[0.6,1.6]
<i>H</i> -dip	<i>K</i> -slope	[[0.493,1],[0.55,1],[0.55,0.875],[0.493,0.875],[0.493,1]]	[0.425,0.55]	[0.875,1.05]
<i>H</i> -dip	<i>H</i> -bump	[[0.493,1.11],[0.55,1.11],[0.55,0.6],[0.493,0.6],[0.493,1.11]]	[0.4,0.54]	[0.6,1.6]

NOTE—Each set of coordinates forms a polygon with 4 or 5 sides.

3.3.1. Strong Candidates

1) WISE J00164397+2304265

This object was first identified following a crossmatch of the PanSTARRS (Kaiser et al. 2010) and WISE (Wright et al. 2010) surveys as a T0 brown dwarf by Best et al. (2015). The *H*-band showed no signs of methane, which is a hallmark of the T dwarf class (Burgasser et al. 1999), but the *J*-band peak resembles that of a T2 dwarf. Thus it was flagged as a spectral binary candidate for its unusual spectrum (Best et al. 2015), finding a closest match with the confirmed L6 + T2 dwarf binary, SDSS J0423–0414 (Burgasser et al. 2005; Geballe et al. 2002). This source has a 93% probability of belonging to the field using parallaxes from Best et al. (2020) in BANYAN Σ (Gagné et al. 2018b).

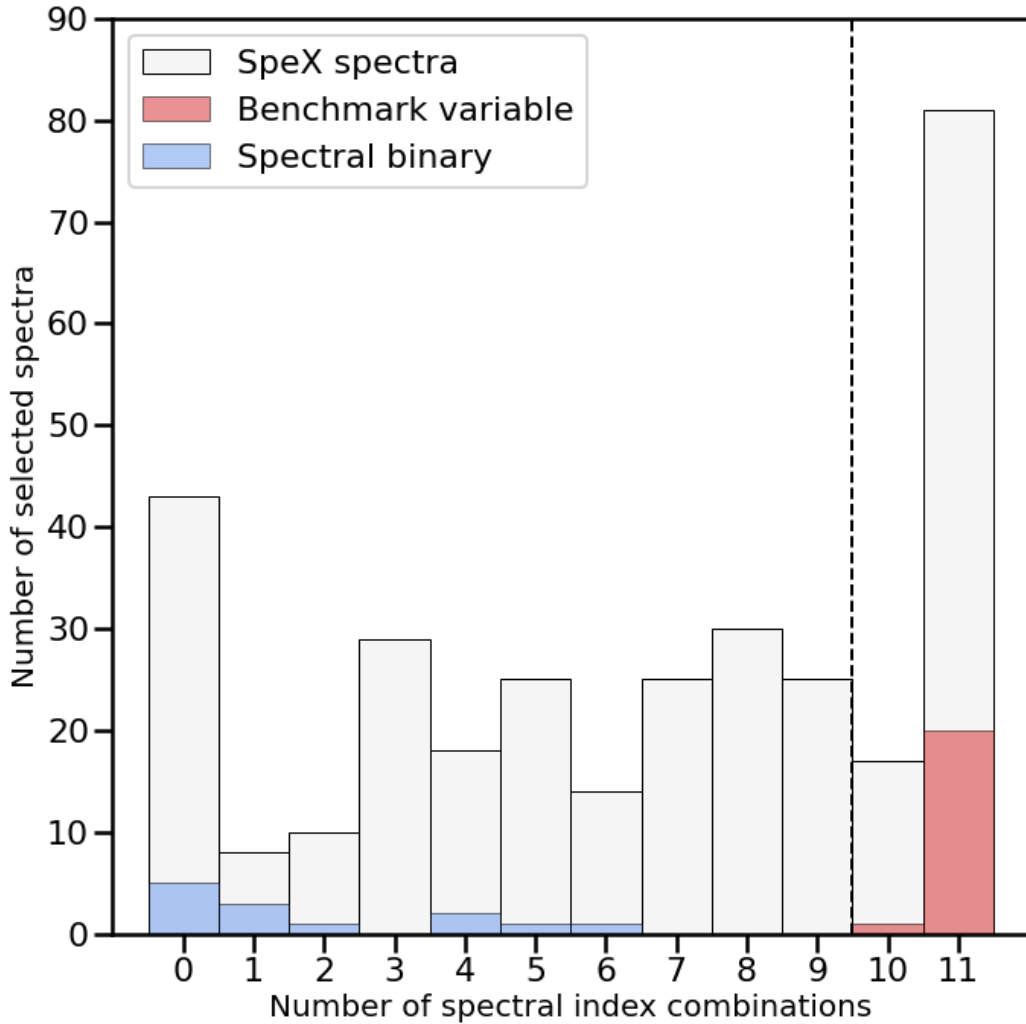


Figure 4. Histogram showing the number of times a spectrum falls in one of our selection regions. Benchmark variables are shown in red, confirmed spectral binaries in blue, and the rest of the spectral sample in gray. The final candidates are the sources found in 10 or more parameter spaces, as shown by the dashed line.

2) 2MASS J00310928+5749364

2MASS J0031+5749 was classified as an L9 brown dwarf by [Best et al. \(2013\)](#) using spectral indices from [Burgasser et al. \(2006a\)](#). This source has a 88% membership probability in Carina Near according to BANYAN Σ ([Gagné et al. 2018b](#)) with kinematic measurements from [Best et al. \(2015\)](#), giving it an age estimate of $13.3_{-0.6}^{+1.1}$ Myr ([Booth et al. 2021](#)). This source was independently monitored for variability with the *Spitzer Space Telescope* and found to be variable by [Vos et al. \(2022\)](#), who measured an amplitude of $0.35 \pm 0.03\%$ at [3.6] and a period of 1.64 ± 0.01 h. The SPL contains two spectra of this object, both found in all 11 index-index regions.

3) 2MASS J02062493+2640237

The J -band spectrum of this object matches that of an L9 dwarf, but the H and K -bands are unusually red, such that it was classified as an L9pec by Kirkpatrick et al. (2011). This object is a part of a rare class of L dwarfs that are red for reasons not attributable to low gravity and appear to have older kinematics than field L dwarfs (Kirkpatrick et al. 2011). This object has a 66.9% probability of belonging to the field according to BANYAN Σ .

4) WISE J023038.90-022554.0

This object was classified as a peculiar L8 dwarf by Thompson et al. (2013) using spectral standards from Kirkpatrick et al. (2010), who noted the object's H -band divot near $1.6 \mu\text{m}$ as well as methane at $2.2 \mu\text{m}$, which are typically indicative of an unresolved T dwarf companion. Thompson et al. (2013) suggested that this spectrum could better be explained as a spectral binary of L7 and T2 components instead of a singular L8 object, however no high resolution imaging exists of this object. According to BANYAN Σ (Gagné et al. 2018b), this object has a 48.6% membership probability in the Hyades (an age of 625 ± 0.5 Myr; Brandt & Huang (2015)) and 34.3% in Carina Near ($13.3^{+1.1}_{-0.6}$ Myr).

5) 2MASS J03264225-2102057

The NIR spectrum of this object was noted by Cruz et al. (2007) to be redder than typical for its spectral type and therefore younger than 500 Myr. Gagné et al. (2015b) later classified 2MASS J0326-2102 as an L5 β , the β signifying intermediate surface gravity. This object is also a high likelihood member of the AB Doradus moving group (130 ± 20 Myr; Barrado y Navascués et al. (2004)). 0326-2102 shows a variability amplitude of $0.34\% \pm 0.04$, albeit a long period of $32.84^{+4.69}_{-4.62}$ h, in the *Spitzer* survey of Vos et al. (2022).

6) 2MASS J06420559+4101599

This object is an unusually red L9 dwarf. Using solely the J -band, this object would result in a T spectral type but shows no sign of CH₄, so the redness could result from a dusty photosphere. It was classified as a medium binary candidate by Best et al. (2015) using criteria from Burgasser et al. (2010). This object was given a 78.6% probability of membership in the AB Doradus Moving Group by the BANYAN II online tool (Gagné et al. 2015a), yet updated with BANYAN Σ to 86% membership probability in AB Doradus (Vos et al. 2022) and thus an age of approximately 130 ± 20 Myr. This source has been confirmed as a photometric variable in the *Spitzer* survey of Vos et al. (2022) with an amplitude of $2.16 \pm 0.16\%$ in *Spitzer* and period of 10.11 ± 0.06 h.

7) 2MASS J06522224+4127366 (PSO J103.0927+41.4601)

Using spectral standards from Burgasser et al. (2006a), this object was classified as a T0.5. However, Best et al. (2013) discovered that this object is a close spectral match to the L6+T2 binary SDSS J0423-0414AB, one of the known variable objects

for which only the blended light spectrum was available in our spectral library. This is a field source based on BANYAN Σ .

8) SDSS J075840.33+324723.4

This source was selected as a weak spectral binary candidate of T0.0+T3.5 dwarf components by Burgasser et al. (2010). It is classified as a T2 dwarf from its SpeX spectrum (Knapp et al. 2004), being only slightly bluer in the J -band than its best-fit single template. *HST* imaging did not resolve this source into two components (Burgasser et al. 2006b). SDSS J0758+3247 has a 93.9% membership probability in Carina Near ($13.3_{-0.6}^{+1.1}$ Myr) according to BANYAN Σ (Gagné et al. 2018b) and a $4.8 \pm 0.2\%$ variability amplitude in J -band from a Spitzer Space Telescope variability monitoring campaign (Vos et al. 2020).

9) SDSS J080959.01+443422.2

Chiu et al. (2006) identified this object as an L6 spectral type brown dwarf from Burgasser et al. (2010) standards. Faherty et al. (2016) proposed that this object is an ambiguous member of either the Argus (40 - 50 Myr; Zuckerman (2019)) or AB Doradus (130 ± 20 Myr) moving groups from its spectrum and kinematics. An ambiguous member requires updated astrometric precision as it either appeared to be part of more than one group or could not be differentiated from the field. This object was observed twice with SpeX, with one of its spectra found in all 11 of our 11 index-index regions, while the other one is only found in 10. This source shows a flat light curve in the *Spitzer* survey of Vos et al. (2022).

10) 2MASS J08300825+4828482

2MASS J0830+4828 was classified as an L9.5 object by Schneider et al. (2014) using the L dwarf classification scheme in Kirkpatrick et al. (2010). $H\alpha$ emission was detected in this object by Schmidt et al. (2007), indicative of magnetic activity and suggestive of youth. However, according to BANYAN Σ , this object has a 99.9% probability of having field kinematics. The SPL contains two spectra of this object which were both found in all 11 index-index regions.

11) SDSS J083717.21-000018.0

This object was one of the earliest L/T transition objects discovered (Burgasser et al. 2000) and classified as a T1 brown dwarf. Of note, it is one of a handful of T-dwarfs with $H\alpha$ emission (Kirkpatrick et al. 2008). Its kinematics are consistent with field membership (99.9% probability). This object has 3 spectra in our library, two appearing in all 11 index-index regions, and one in only 10.

12) 2MASS J08503593+1057156

Burgasser et al. (2011) posited that this might be a triple system with an equal mass unresolved binary due to the fact that one of the objects was twice as bright as the other despite being of the same spectral type. Later, Faherty et al. (2011) identified a potential binary comover. The SpeX spectrum of 2MASS J0850+1057 was later

modeled as a $L6.5\pm 1$ and $L8.5\pm 1$ spectral binary and the comover was disproved with more precise astrometry (Dupuy & Liu 2012). However, HST photometry for this object (Brock et al. 2021) suggested the large differences in component brightness across several bands hinted that the A component is indeed a binary itself, as originally suggested by Burgasser et al. (2011). This object was also originally thought to have signatures of youth, but Gagné et al. (2015b) concluded that it is most likely a field object, positing that its unusually red spectrum could be explained by the presence of thicker/higher clouds in the atmosphere. There are 2 spectra of this system in our SpeX Prism Library, both of them appearing in all 11 index-index regions.

13) SDSS J085234.90+472035.0

Using the L dwarf classification scheme developed by Kirkpatrick et al. (2010), this object was classified as an L9.5 dwarf (Schneider et al. 2014). While thought to potentially belong to a young moving group (Gagné et al. 2015b), with the updated BANYAN Σ it has 99.9% probability of being part of the field. Manjavacas et al. (2016) identified SDSS J0852+4720 as a weak candidate for spectral binarity of L7+T1 dwarf components using the spectral indices from Bardalez Gagliuffi et al. (2014) and Burgasser et al. (2010).

14) SDSS J093109.56+032732.5

SDSS J0931+0327 is unusually blue for its spectral type of L7.5 (Knapp et al. 2004). According to BANYAN Σ , this object has a 89.9% probability of belonging to the Carina Near moving group ($13.3_{-0.6}^{+1.1}$ Myr). Using cloud models, Knapp et al. (2004) calculated that its unusually blue colors might indicate a high sedimentation efficiency and a low cloud optical depth. Radigan et al. (2014) obtained a light curve for this object as a part of a variability survey and did not detect significant variability. They detected a peak to peak variability amplitude of 0.041%, which was not significant as the white noise estimate for the relative-flux light curve was 0.036%. This object was identified as a spectral binary candidate by Bardalez Gagliuffi et al. (2015) through visual inspection, yet an adaptive optics image with Keck/NIRC2 did not reveal a secondary companion (Bardalez Gagliuffi et al. 2015).

15) 2MASS J09553336-0208403

2MASS J0955-0208 is a known young L7 brown dwarf (Gagné et al. 2017b), although its membership probabilities point to 55.5% for field and 33.5% for AB Doradus (130 ± 20 Myr). This object has a very red $J - K$ color, a triangular-shaped H -band continuum, and weak K I absorption lines, which are all indicative of low surface gravity.

16) 2MASS J09560810-1447065

Best et al. (2015) classified this brown dwarf as an L9 type using visual comparisons with field standards and a $T0.0\pm 0.5$ type brown dwarf using index-based classification. They flagged this object as a medium binary candidate because of subtle signs of methane absorption indicative of a T-dwarf using the spectral indices method (Bur-

gasser et al. 2010; Bardalez Gagliuffi et al. 2014). 2MASS J0956-1447 is a known field object (Schneider et al. 2017).

17) 2MASSI J1043075+222523

Cruz et al. (2007) discovered this object and performed an optical spectroscopy follow-up of this object and classified it as an unusually red L8 dwarf. They provided the possible explanation that the object was an unresolved spectral binary as a reason for its peculiar spectrum. 2MASS J1043+2225 is classified as an intermediate gravity object with the scheme from Allers & Liu (2013). This object has measured H α emission (Pineda et al. 2016) and a measured rotation period of $2.21^{+0.14}_{-0.13}$ hours in 8-12 GHz radio frequencies (Kao et al. 2018).

18) Luhman 16A (WISE J104915.57–531906.1A)

Luhman 16A was discovered in 2013 by Luhman (2013) using multi-epoch astrometry from the Wide-field Infrared Survey Explorer (WISE), as one component of a 3 AU separated flux reversal binary, meaning that the two components switch in relative brightness at different bands. The B component is brighter at J , but fainter in the K band, which is a phenomenon that can potentially be explained by thick clouds (Burgasser et al. 2013). Luhman16AB is located at 1.9980 ± 0.0004 pc, making it the third closest system to the Sun after Alpha Centauri ($d = 1.3475 \pm 0.256025$ pc; Henry et al. 2018) and Barnard’s star ($d = 1.8282 \pm 0.00013$ pc; Lindegren et al. 2021). Burgasser et al. (2013) classified this object as an $L7.5 \pm 0.9$ spectral type brown dwarf, and its companion as a $T0.5 \pm 0.7$ dwarf using indices and spectral type/index relations (Geballe et al. 2002; Burgasser et al. 2006a; Burgasser 2007a). Luhman 16A is one of the reddest L dwarfs known ($J - K = 2.08 \pm 0.08$ mag, Burgasser et al. 2013), suggestive of thick cloud coverage (Faherty et al. 2014).

The individual components of Luhman 16 have been monitored for variability multiple times in the past. Buezli et al. (2015b) used *HST*/WFC3 at $1.1\text{--}1.66 \mu\text{m}$ for spectroscopic variability and found an upper limit for Luhman 16A of 0.4%, whereas the B component showed variability amplitudes of 7-11% changing within a single rotation period. Later *HST*/WFC3 observations in the $0.8\text{--}1.15 \mu\text{m}$ range found a 4.5% amplitude in Luhman 16A (Buezli et al. 2015a). Using TESS data of the system, the period of Luhman 16A was determined to be 6.94 hours, and this periodicity is much lower amplitude than that of the B component (Apai et al. 2021). Mutli-wavelength photometric monitoring with the 2.2-m MPG/ESO GROND telescope covering $rizJHK$ bands found 2% and 3% variability amplitudes for Luhman 16A in i and z bands, respectively (Biller et al. 2013). However, no variability was detected in r -band or the NIR JHK bands. The NIR spectrum of Luhman 16A can be modeled with an intermediate thickness, single cloud layer at 1200 K (Buezli et al. 2015b). The B component of this binary system is a known variable brown dwarf and a benchmark variable in our analysis.

19) 2MASS J11193254-1137466

2MASS J1119-1137 or TWA 42 is one of the reddest sources known with a $J - K$ color of 2.62 ± 0.15 mag (Kellogg et al. 2015). This source is a high likelihood member of the 10 Myr old TW Hydrae association according to its kinematics and spectra (Faherty et al. 2016). However, updated kinematics yield a BANYAN Sigma estimate of 63.2% probability of field membership (Best et al. 2020). TWA 42 was discovered to be an approximately equal magnitude binary of L7 dwarfs with a separation of $0''.14$ (3.6 ± 0.9 AU; Best et al. 2017). Both components are among the lowest-mass brown dwarfs in the solar neighborhood ($M \approx 4M_{\text{Jup}}$). Schneider et al. (2018) performed time-series photometry of this object with *Spitzer* [3.6] and [4.5] bands and found low amplitude variability of $0.230^{+0.036}_{-0.0035}\%$ and $0.453 \pm 0.037\%$, respectively, but could not quantify the effects of binarity on the system’s rotational parameters.

20) SDSS J121951.45+312849.4

SDSS J1219+3128 is an L9 dwarf (Schneider et al. 2014), and known variable from the *Hubble Space Telescope* Near-Infrared Spectroscopic Survey for variability, but it only has a lower limit for variability ($> 2\%$) as they were not able to observe the full period (Buenzli et al. 2014). Therefore we did not include it in our benchmark variable objects. Manjavacas et al. (2019) searched for whether confirmed photometrically variable objects also were candidates for having composite spectra using the Burgasser et al. (2010) and Bardalez Gagliuffi et al. (2014) techniques and found that it was a strong spectral binary candidate with a best matching fit of an L8 and T4 ($\Delta T_{\text{eff}} \approx 200$ K).

21) SDSSp J125453.90-012247.4

SDSSp J1254-01222 is a T2 dwarf with weak $H\alpha$ emission at 6563 \AA (Burgasser et al. 2003). Metchev et al. (2015) detected an upper limit of variability for this object of $< 0.15\%$ at [3.6] and $< 0.3\%$ at [4.5] with *Spitzer*, which is very low-level variability. This object is also a field age dwarf (Filippazzo et al. 2015).

22) DENIS J132620.0-272936

DENIS J1326-2729 is an L5 dwarf in the optical (Gizis 2002) and an L7 in the NIR. This object has a spectrum sloped towards red wavelengths and a characteristic peaked H -band suggesting youth. While this object has been flagged as a potential member of the Argus young moving group (Gagné et al. 2015b) meaning an age estimate of 40 - 50 Myr, BANYAN Σ gives an 88% probability of membership in Carina Near ($13.3^{+1.1}_{-0.6}$ Myr).

23) SDSS J133148.92-011651.4

SDSS J1331-0116 is an L8 brown dwarf in the infrared with unusually blue colors for its spectral type, similar to another candidate SDSS J0931+0327 (Knapp et al. 2004), potentially due to low metallicity. Its atypical spectral features usually point to a blend of binary compositions, but Best et al. (2021) calculated a binary spectral decomposition of L6+T5 with $\Delta J = 1.97 \pm 0.18$ mag which is much larger than the observed magnitude difference of 0.6 mag, making it unlikely that the peculiarity is

due to binarity. This object has three observations in the SPL, which were all found in all 11 index-index regions.

24) 2MASS J15164306+3053443

This object is a weak spectral binary candidate with no high resolution imaging (Burgasser et al. 2010; Bardalez Gagliuffi et al. 2015), potentially composed of an L8+L9.5 dwarfs. However, the binary template fitting of Burgasser et al. (2010) could not rule out the possibility that this object was single with an unusual atmosphere. 2MASS J1516+3053 is also a confirmed variable object from *Spitzer* (Metchev et al. 2015) with amplitudes of $2.4 \pm 0.2\%$ at [3.6] and $3.1 \pm 1.6\%$ at [4.5] bands and a period of 6.7 hr.

25) 2MASSW J1632291+190441

2MASSW J1632+1904 is one of the earliest discovered late L dwarfs (L8, Reid et al. 1999), and identified as a weak binary candidate by Burgasser et al. (2010). Metchev et al. (2015) found this object to have amplitudes of $0.42 \pm 0.08\%$ at [3.6] and $0.5 \pm 0.3\%$ at [4.5] and a period of 3.9 ± 0.2 hr, and thus we did not use it as a benchmark variable due to its low-level variability ($< 1\%$). This object contains two spectra in the SPL.

26) WISE J164715.57+563208.3

This L9 brown dwarf is unusually red with $J - K = 2.20 \pm 0.10$ mag. In a red optical survey with Keck/LRIS, Pineda et al. (2016) obtains optical spectra for WISE J1647+5632 and suggests that it is an unresolved binary system from its spectra. This object is unlikely to be young from its proper motion, photometric distance estimate, and spectrum (Schneider et al. 2017). This source has been independently confirmed as variable by the *Spitzer* survey of Vos et al. (2022) with an amplitude of $0.47 \pm 0.06\%$ and period of $9.234_{-0.25}^{+0.23}$ hours.

27) WISE J173859.27+614242.1

WISE J1738+6142 was discovered in 2013 with WISE. This object is a late L/early T, but it defies a standard spectral classification because of its highly unusual spectrum (Mace et al. 2013). It has excess flux on the blue side of the H and K bands, hinting at a T dwarf secondary and is thought to have rapid changes in atmospheric conditions.

28) 2MASS J17410280-4642218

This object is an L5 dwarf and was noted to likely be a member of β -Pic or AB Doradus moving groups (Faherty et al. 2016). 2MASS J1741-4642 is now a confirmed member of AB Dor (Kirkpatrick et al. 2021) and thus 130 ± 20 Myr old. Vos et al. (2019b) observed this object for photometric variability using the New Technology Telescope (NTT) and the United Kingdom Infrared Telescope (UKIRT) using the J_S band (1.16 - $1.32 \mu\text{m}$), but did not observe any variability. However, the NTT observation was of short duration and therefore amplitudes would have had to be greater than 10% to detect significant variations. This source has been confirmed as

a photometric variable in the *Spitzer* survey of Vos et al. (2022) with an amplitude of 0.35 ± 0.03 and period of $15_{-0.57}^{+0.71}$ hours.

29) WISEP J183058.57+454257.9

This object was first identified by Kirkpatrick et al. (2011) with WISE and classified as an L9 dwarf. It was identified as a medium binary candidate (Best et al. 2015) using the criteria from Burgasser et al. (2010), showing signs of methane absorption.

30) WISE J185101.83+593508.6

WISE J1851+5935 was classified as L9 when evaluated as a single template (Best et al. 2013). However, the *H* and *K*-band peaks have lower flux than typical L9 standards (Kirkpatrick et al. 2010). Thompson et al. (2013) analyzed this spectrum as an unresolved binary, and found that it was better fit as an L7 and T2 binary than as a single source. However, WISE J1851+5935 does not appear as a spectral binary candidate in Burgasser et al. (2010) or Bardalez Gagliuffi et al. (2014).

31) 2MASSW J2101154+175658

This object was discovered by Kirkpatrick et al. (2000). It was identified as a binary system by Bouy et al. (2003) and composed of L7 and L8 dwarfs (Dupuy & Liu 2012). 2MASSW J2101+1756 is a potential member of the Scorpius Centaurus Complex (SCC) (Gagné et al. 2015b) which is ~ 10 Myr old (Song et al. 2012), but the updated Banyan Σ gives a 56% field probability. There are two spectra of this object in the SPL.

32) 2MASS J21243864+1849263

From a crossmatch of SDSS, 2MASS, and WISE, 2MASS J2124+1849 was identified as an L-dwarf with unusual red colors that could suggest low surface gravity or unusual dust content and cloud properties. (Kellogg et al. 2015). According to BANYAN Σ , this object has a 79.7% membership probability in Carina Near $13.3_{-0.6}^{+1.1}$ Myr.

33) 2MASS J21315444-0119374

This object was identified from imaging data of the Sloan Digital Sky Survey (SDSS) (Chiu et al. 2006). Schneider et al. (2014) classified this object as an L9.5 in the near infrared using the L dwarf classification scheme found in Kirkpatrick et al. (2010). This object is a widely separated common proper motion companion of the low-mass stars NLTT 51469AB, which is a close binary of M3 and M6 components (Gauza et al. 2019).

34) 2MASS J22153705+2110554

2MASS J2215+2110 was discovered very recently by Kellogg et al. (2015), as it was previously overlooked in SDSS. This T0.0 dwarf is only a weak candidate binary using the indices from Burgasser et al. (2010), but it has a peculiar spectrum and a lack of flux in the *H*-band compared to other early T dwarfs. Eriksson et al. (2019) identified this object as a strong variable with a $10.7 \pm 0.4\%$ amplitude in the *J* band and noted

that it seems unlikely that this object is an unresolved binary system as previously suggested. We did not include this object as one of our benchmark objects, because it was discovered to be variable after the curation of our benchmark list. However, the SPL contains two observations of this object both found in all 11 index-index regions.

35) 2MASS J22443167+2043433

This object is an L6 spectral type brown dwarf (Faherty et al. 2016). 2MASS J2244+2043 is a bona fide member of AB Doradus (Faherty et al. 2016) meaning that it is 130 ± 20 Myr old. Morales-Calderón et al. (2006) detected sinusoidal variability with a period of 4.6 hours for this object using the Spitzer/IRAC $4.5 \mu\text{m}$ and $8 \mu\text{m}$ band passes. Vos et al. (2018) identified a longer period of 11 ± 2 h with *Spitzer* light curves, seeing a variability amplitude of $0.8 \pm 0.2\%$ in [3.6]. However, Vos et al. (2019b) observed a $5.5 \pm 0.6\%$ variability amplitude in *J*-band. The change in period is most likely due to the short observing window of 8.2 h in Morales-Calderón et al. (2006).

36) WISE J232728.74-273056.6

WISE J2327-2730 is an L9 object with slightly redder WISE colors than usual (Kirkpatrick et al. 2011). They suggest that low gravity would cause the NIR spectrum to be unusually red. They also eliminate the possibility that the peculiarity arises from binarity, because the estimated companion would have to be a T6.5 dwarf, which would cause a much more peculiar NIR spectrum. Thus, the peculiarity in color is unexplained, and we propose it might be due to cloud-driven variability.

37) WISE J233527.07+451140.9

This object was discovered by (Thompson et al. 2013) and visually classified as an L7 dwarf (Liu et al. 2016). Gagné et al. (2014) identified this object as an old field candidate with a 97% probability using BANYAN II, confirmed by BANYAN Σ (99.9% field probability). WISE J2335+4511 is a very red peculiar brown dwarf that does not show signs of weaker K I lines expected in a low gravity object (Thompson et al. 2013), so it is a part of a class of brown dwarfs that are unusually red objects that are not young.

3.3.2. Weak Candidates

1) 2MASSI J0028394+150141

2MASSI J0028+1501 is an unusually red mid L dwarf. Knapp et al. (2004) suggests that the redness could be due to variability between 5 – 10%. However, no follow-up photometry exists for this object. This source has a 91% membership probability in Argus according to BANYAN Σ .

2) DENIS J025503.3-470049

DENIS J0255-4700 is an L9 brown dwarf (Schneider et al. 2014). Variability was not detected in red optical bands *I* and *R* in a search by Koen (2005).

3) 2MASSI J0328426+230205

2MASSI J0328+2302 is an L9.5 spectral type brown dwarf (Knapp et al. 2004). A NIR variability amplitude of 0.43 ± 0.16 mag was detected in this object by Enoch et al. (2003), but they were unable to differentiate whether this variability was intrinsic to the brown dwarf or the comparison star. When later observed by Radigan et al. (2014), they found no significant variability in the target over a 3.7 hr observation. Burgasser et al. (2010) noted that this object is overluminous for its spectral type, therefore could be an unresolved binary system.

4) SDSS J085834.42+325627.7

This object was first identified by Chiu et al. (2006) as a T1 dwarf. Photometric monitoring set variability upper limits of $< 0.27\%$ at [3.6] and $< 0.64\%$ at [4.5] (Metchev et al. 2015). SDSS J0858+3256 is unusually red with a large tangential velocity ($V_{tan} = 66 \pm 3 \text{ km s}^{-1}$; Faherty et al. (2009)) and a 99.9% probability from BANYAN Σ of being a field object.

5) SDSSp J132629.82-003831.5

SDSSp J1326-0038 is an L7 brown dwarf and a candidate member of Argus (40 - 50 Myr) with a 85% probability (Gagné et al. 2015b) from BANYAN II. With the updated BANYAN Σ , however, it has a 100% probability of being a field object. When observed by Radigan et al. (2014), this object only had a 0.047% peak-to-peak amplitude in J -band.

6) WISEA J161628.32+062135.1 (PSO J244.1180+06.3598)

This object was first identified following a crossmatch of the PanSTARRS and WISE surveys as a T0 brown dwarf by Best et al. (2015), although it has also been classified as an unusually red L9 brown dwarf. The spectra shows indication of youth because of redder-than-usual colors and triangular H -band shape. However, this object has an 99.9% probability of belonging to the field from BANYAN Σ .

7) SDSS J175024.01+422237.8

SDSS J1750+4222 is a T1 spectral type brown dwarf (Geballe et al. 2002). This object has a reported light-curve by Radigan et al. (2014). They found a marginal detection of $1.5 \pm 0.3\%$ variability amplitude and a 2.7 ± 0.2 hr period due to quality concerns with the light curve.

8) 2MASS J21522609+0937575

This object was discovered by Reid et al. (2006a). 2MASS J2152+0937 is an equal mass/equal luminosity binary system of L6 spectral type (Reid et al. 2008).

Table 4. Variability candidates with spectral types between L7–T3

Source	Spectral Type	BANYAN Σ	Filter	Variability		Reference
				Amplitude (%)	Youth; Variability; Spectral Binary Candidate	
2MASS J00164364+2304262	T1.0	93% FLD ; ... ; (2)
2MASS J00310928+5749364	L9.0	96% CARN	[3.6]	0.35 ± 0.03	(3) ; (3) ; ...	(3) ; (3) ; ...
2MASS J01020186+0355405	T0.0	98% FLD ; ... ; ...
2MASS J02062493+2640237	L8.0	67% FLD ; ... ; ...
WISE J023038.90-022554.0	L9.0	49% HYA, 34% CARN*	(1) ; ... ; (4)	(1) ; ... ; (4)
2MASS J03185403-3421292	L8.0	100% FLD ; ... ; ...
WISE J032301.86+562558.0	L7.0	100% FLD ; ... ; ...
† 2MASS J03264225-2102057	L9.0	92% ABDMG	[3.6]	0.34 ± 0.04,	(3) ; (3) ; ...	(3) ; (3) ; ...
† 2MASS J06420559+4101599	L8.0	86% ABDMG	[3.6]	2.16 ± 0.16	(3) ; (3) ; ...	(3) ; (3) ; ...
2MASS J06522224+4127366	T0.0	100% FLD* ; ... ; (5)
† SDSS J075840.33+324723.4	T2.0	94% CARN*	J	4.8±0.2	(1) ; (6) ; (7)	(1) ; (6) ; (7)
SDSS J080959.01+443422.2	L7.0	89% FLD	[3.6]	0.77±0.06 ; (3) ; ...
SDSS J082030.12+103737.0	T0.0	75.5% FLD* ; ... ; ...
2MASSW J0829570+265510	L7.0	50% FLD, 50% ARG*	(1) ; ... ; ...	(1) ; ... ; ...
SDSSp J083008.12+482847.4	T0.0	100% FLD ; ... ; ...
SDSSp J083717.22-000018.3	T1.0	100% FLD ; ... ; ...
2MASSs J0850359+105716	L7.0	51% FLD, 47% CARN	(1) ; ... ; (8), (9)	(1) ; ... ; (8), (9)
SDSS J085234.90+472035.0	T0.0	100% FLD* ; ... (10)
SDSSp J085758.45+570851.4	L8.0	100% FLD ; ... ; ...
2MASSI J0859254-194926	L7.0	98% FLD ; ... ; ...
† 2MASSW J0929336+342952	L8.0	69% ARG*	(1) ; ... ; ...	(1) ; ... ; ...
† SDSS J093109.56+032732.5	T0.0	90% CARN*	J	0.041 ± 0.036	(1) ; (11) ; (12)	(1) ; (11) ; (12)

Strong candidates

Table 4 continued on next page

Table 4 (continued)

Source	Spectral Type	BANYAN Σ	Variability			Reference
			Filter	Amplitude (%)	Youth; Variability; Spectral Binary Candidate	
2MASS J09553336-0208403	L8.0	56% FLD, 34% ABDMG*	(1); ...; ...	
2MASS J09560810-1447065	T0.0	100% FLD*; ...; (2)	
SDSS J100711.74+193056.2	L9.0	86% ARG*	(1); ...; ...	
2MASS J10430758+2225236	T0.0	100% FLD*; ...; (13)	
WISE J104915.57-531906.1A	L9.0	89% ARG	J	4.5%	(1); (20); ...	
2MASS J11193254-1137466	L7.0	63.2% FLD	[3.6], [4.5]	$0.230^{+0.036}_{-0.0035}$, 0.453 ± 0.037	...; (14); ...	
† 2MASS J12010443+5730040	T0.0	71.1% UMA*	(1); ...; ...	
SDSS J121951.45+312849.4	T0.0	100% FLD*	J	> 2	...; (15); ...	
SDSSp J125453.90-012247.4	T2.0	100% FLD	[3.6], [4.5]	< 0.15, < 0.36	...; (16); ...	
† 2MASSW J1326201-272937	L7.0	88% CARN	(1); ...; ...	
SDSS J133148.92-011651.4	T0.0	100% FLD; ...; ...	
WISE J151314.61+401935.6	L9.0	100% FLD*; ...; ...	
SDSS J151506.11+443648.3	L7.0	100% FLD*; ...; ...	
SDSS J151643.01+305344.4	T2.0	83% FLD*	[3.6], [4.5]	2.4 ± 0.2 , 3.1 ± 1.6	...; (16); ...	
SDSS J154009.36+374230.3	L9.0	100% FLD*; ...; ...	
SDSS J163030.53+434404.0	L9.0	100% FLD*; ...; ...	
2MASSW J1632291+190441	L8.0	100% FLD	[3.6], [4.5]	0.42 ± 0.08 , 0.5 ± 0.3	...; (16); (7)	
WISE J164715.57+563208.3	L8.0	66% FLD	[3.6]	0.47 ± 0.06	(3); (3); ...	
WISE J173859.27+614242.1	L7.0	83% FLD*; ...; ...	
† WISE J174102.78-464225.5	L7.0	99% ABDMG	[3.6]	0.35 ± 0.03	(3); (3); ...	
WISE J183058.56+454257.4	L9.0	92% FLD*; ...; (2)	
2MASS J18510178+5935040	L9.0	100% FLD; ...; (4)	
2MASSW J2101154+175658	L8.0	56% FLD; ...; ...	
† 2MASS J21243864+1849263	T0.0	80% CARN*	(1); ...; ...	
SDSS J213154.43-011939.3	L9.0; ...; ...	
2MASS J22153705+2110554	T0.0	...	J	10.7 ± 0.4	...; (7); (17)	
† 2MASSW J2244316+204343	L7.0	100% ABDMG	J	5.5 ± 0.6	(1); (18); ...	

Table 4 continued on next page

Table 4 (*continued*)

Source	Spectral Type	BANYAN Σ	Variability			Reference
			Filter	Amplitude (%)	Youth; Variability; Spectral Binary Candidate	
WISE J232728.74-273056.6	T0.0 ; ... ; ...	
2MASS J23352734+4511442	L7.0	100% FLD ; ... ; ...	
<i>Weak candidates</i>						
† 2MASS J0028394+150141	L7.0	91% ARG*	(1) ; ... ; ...	
SDSSp J003259.36+141036.6	L9.0	62% FLD, 38% CARN	(1) ; ... ; ...	
WISE J02022929+2305139	L7.0	72% ARG*	(1) ; ... ; ...	
DENIS J025503.3-470049	L9.0	100% FLD	JHK	flat	... ; (19) ; ...	
2MASS J0328426+230205	T0.0	100% FLD	J	0.013	... ; (11) ; (7)	
SDSS J073922.26+661503.5	T2.0	100% FLD* ; ... ; ...	
SDSS J085834.42+325627.7	T0.0	100% FLD*	[3.6], [4.5]	< 0.27, < 0.64	... ; (16) ; ...	
SDSSp J132629.82-003831.5	L7.0	100% FLD	J	0.047	... ; (11) ; ...	
WISEA J161628.32+062135.1	L7.0	100% FLD ; ... ; ...	
SDSS J175024.01+422237.8	T2.0	60% ARG, 40% FLD*	J	2.7±0.2	(1) ; (11) ; ...	
2MASS J21522609+0937575	L7.0	100% FLD* ; ... ; ...	

Table 4 *continued on next page*

Table 4 (*continued*)

Source	Spectral Type	BANYAN Σ	Variability			Reference
			Filter	Amplitude (%)	Youth; Variability; Spectral Binary Candidate	

References—(1) This paper; (2) Best et al. (2015); (3) Vos et al. (2022); (4) Thompson et al. (2013); (5 - Best et al. (2013); (6) Vos et al. (2020); (7) Burgasser et al. (2010); (8) Burgasser et al. (2011); (9) Brock et al. (2021); (10) Manjavacas et al. (2016); (11) Radigan et al. (2014); (12) Bardalez Gagliuffi et al. (2015); (13) Cruz et al. (2007); (14) Schneider et al. (2018); (15) Buenzli et al. (2014); (16) Metchev et al. (2015); (17) Eriksson et al. (2019); (18) Vos et al. (2019b); (19) Koen et al. (2005); (20) Buenzli et al. (2015a)

NOTE—In this table we summarize the literature research on all 62 of our candidates. The spectral type is the spectral type designated by the SpeX spectral classifications. For youth, we provide the BANYAN Σ probability of belonging to a young moving group (FLD - field; CARN - Carina Near; ABDMG - AB Doradus; ARG - Argus; UMA - Ursa Major). For objects with previous variability monitoring, we designate the wavelength of the observations and the amplitude of the modulations. Lastly, when available we provide the reference to papers that comment on spectral binary candidacy of any of our objects. Refer to section 3.1 for a discussion of notable candidates.

† These objects are young based on our classifications which come from both moving group association and spectral indicators of youth in the literature.

* These objects do not have measured parallaxes.

3.4. Contamination by spectral binaries

Blended-light spectra can have a binary origin (Burgasser et al. 2010; Bardalez Gagliuffi et al. 2014) or be the consequence of patchy atmospheric layers at various temperatures, as shown in this study. In order to estimate the contamination fraction of variability candidates by spectral binaries, we modeled synthetic spectral binary systems and applied our variability detection technique on them. We use our entire spectral library of 325 spectra of L7–T3 dwarfs and applied the Burgasser et al. (2010) technique which is designed to identify T dwarf companions to L7-T3 dwarf primaries. Following this analysis, we remove 87 spectra from 76 sources from our library, which we identify as spectral binary candidates from the Burgasser et al. (2010) technique, many of which have been already confirmed with high resolution follow-up observations. The confirmed and candidate spectral binaries are listed in Table A.2 for further reference. These spectra, as well as spectra from confirmed variables and our variability candidates, were removed from our sample leaving 147 presumably single, non-variable spectra.

We generated spectral binary templates by interpolating all remaining spectra onto a common wavelength range and then adding every two spectra together. In total, we generated 10731 spectral binary templates, which were all classified according to the Kirkpatrick et al. (2010) prescription. Finally, we apply our variability detection technique on this sample of synthetic spectral binaries. We found that only 2.3% of synthetic spectral binaries were selected as weak variability candidates, and an additional 2.3% as strong variability candidates, amounting to a total 4.6% contamination rate of our variability technique by true spectral binaries with similar spectral features as those flagged by our technique. These features could be dependent on the effective temperature of the object, cloud composition, cloud coverage fraction, strength of vertical transport to name a few variables.

As a complement, we can also provide a rough estimate of the number of candidate and confirmed spectral binaries from our list of 62 variability candidates. We find that 2MASS J0850+1057 is a confirmed closely-separated binary system, whose unresolved spectrum is best fit by a binary template of nearly equal flux components, hence not considered a spectral binary. Six other objects are candidate spectral binaries. However, upon closer inspection, we find that 2 of them are not selected by either the Burgasser et al. (2010) or the Bardalez Gagliuffi et al. (2014) spectral binary techniques: WISE J0016+2304 was selected only by indices (Best et al. 2015) and WISE J0230–0225 identified as a potential binary by visual inspection (Thompson et al. 2013). Two other sources, SDSS J0758+3247 and SDSS J0931+0327, do not show any companion on high resolution follow-up (Burgasser et al. 2010 and Bardalez Gagliuffi et al. 2014, respectively). Finally, 2MASS J1516+3053 and SDSS J1219+3128 are spectral binary candidates, yet both previously tagged to have unusual atmospheric properties (Burgasser et al. 2010 and Manjavacas et al. 2019, respectively). This spot check on spectral binaries within our variability candidate list further suggests

that our index-based technique will have little contamination from spectral binary systems.

4. DISCUSSION

4.1. Variability Fractions

Table 5. Comparison of variability fractions with the literature

Sample	This Paper	Radigan et al. (2014)	Metchev et al. (2015)
L7–T3 spectral type range			
Total sources	270	25	16
Confirmed variables	15	5	7
Candidates	62
Variability Fraction	$5^{+2}_{-1}\%$	$19^{+11}_{-9}\%$	$43^{+26}_{-17}\%$
Variability Fraction (inc. cand. a)	$21 \pm 3\%$
L9–T3 spectral type range			
Total sources	140	15	12
Confirmed variables	9	5	4
Candidates	37
Variability Fraction	$6 \pm 2\%$	$33^{+21}_{-16}\%$	$33^{+25}_{-18}\%$
Variability Fraction (inc. cand. a)	$24^{+5}_{-4}\%$

NOTE—For the variability fraction including candidates, we consider both strong and weak candidates.

a This fraction assumes that the total number of variables is the number of benchmarks plus 67% of the variability candidates. These fractions increase to $28^{+4}_{-3}\%$ and $33^{+6}_{-5}\%$ for L7–T3 and L9–T3 spectral type ranges, respectively, if 100% of candidates were to show significant variability amplitudes.

In order to assess the success of our technique in predicting variability, we compare variability fractions including our candidates with results from variability surveys from the literature. However, as discussed in Section 3.1, it is important to note that surveys carried out at different wavelengths and with different instruments achieve a wide range of precision and variability amplitudes which differ as a function of wavelength. The comparisons presented here should be interpreted as a rough check of the proportion of candidate variables obtained using our variability indices.

Within our sample of 270 L7–T3 dwarfs (most of which lack photometric monitoring observations), we used 15 sources as benchmark variables, leading to a raw variability fraction of $5^{+2}_{-1}\%$ with asymmetrical uncertainties representing the central 68% of a Poisson distribution (see Table 5). Radigan et al. (2014) obtained ground-based light curves in J -band for 62 L4–T9 brown dwarfs. From their study, we calculate a raw variability fraction of $19^{+11}_{-9}\%$ (5/25) in the L7–T3 range that we focus on for this work. Our raw variability fraction is at least 1σ lower than the one from Radigan et al. (2014) because only a small part of our sample has been followed up with photometric

monitoring. Similarly, [Metchev et al. \(2015\)](#) obtained *Spitzer* light curves in [3.6] and [4.5] bands for 44 L3–T8 dwarfs. Within the L7–T3 range, they find 7 variable sources out of 16, leading to a raw fraction of $43_{-18}^{+24}\%$. This fraction is significantly higher than the ground-based fractions from [Radigan et al. \(2014\)](#) and our study because *Spitzer* is more sensitive to low-level variability amplitudes.

A comprehensive photometric monitoring follow-up survey of our candidates is needed to determine the false positive rate of our technique. Among the strong candidates, 14 have previous light curves (including 4 from the new *Spitzer* survey of [Vos et al. \(2022\)](#)). Of these, 12 objects have a significant amplitude, whereas 2 do not show significant variability in this wavelength range. From the weak candidates, 4 have previous light curves, none of which exhibit significant variability. Therefore, from this preliminary assessment, it is likely that 67% (12/18) of our candidates will show significant light curve amplitudes after photometric monitoring. Our technique would return almost three times as many significantly variable light curves for L/T transition sources as a randomly-selected sample, using the independent analysis of the near-infrared Brown dwarf Atmosphere Monitoring survey by [Radigan \(2014\)](#) as a comparison ($24_{-9}^{+11}\%$ for L7–T3.5 dwarfs). If this trend continues, 67% of our 62 of our variability candidates should show significant variability, and our variability fraction would increase to $21 \pm 3\%$, which is comparable to the upper limit of [Radigan et al. \(2014\)](#). However, in order to fully describe our confusion matrix, we would need to homogeneously obtain NIR light curves for every object in our sample, in order to evaluate the effectiveness of our selection technique at identifying those light curves showing significant variability.

[Radigan et al. \(2014\)](#) also carried out a focused analysis on 16 L9–T3.5 dwarfs, out of which 4 had variable light curves, arriving at a fraction of $39_{-14}^{+16}\%$ after correcting for their sensitivity to astrophysical signals. Since our spectral type range technically only goes to T3, we recalculated the [Radigan et al. \(2014\)](#) variability fraction for L9–T3 dwarfs (excluding one T3.5 from their sample) and obtain $33_{-16}^{+21}\%$. We find the same fraction for the [Metchev et al. \(2015\)](#) sample reduced accordingly to L9–T3, $33_{-18}^{+25}\%$. Within this spectral type range, our raw variability fraction is $6 \pm 2\%$ for confirmed variables.

4.2. Atmospheric Structure: Bands, Spots, Inclination Effects

Variability in a brown dwarf light curve is caused by a heterogeneous cloud coverage of its atmosphere, implying that each longitudinal slice has a different brightness. This difference in brightness in L/T transition objects is probably due to patchy clouds in the atmosphere ([Ackerman & Marley 2001](#)). However, not all cloud structures result in variability. If a brown dwarf has zonally or longitudinally symmetric atmospheric cloud features, it will have a flat light curve as the brightness remains the same during the rotation period. Within the solar system, cloud-banding can be seen in Jupiter. Jupiter’s banded structure is caused by belts, dark colored bands,

and zones, light colored bands. The bands of Jupiter display some variability, but the bulk features remain relatively constant (Ge et al. 2019). Atmospheric dynamical simulations show that zonal banding likely occurs for brown dwarfs and giant exoplanets (Tan & Showman 2021b). Our technique, which probes the spectra, may be sensitive to blended-light signatures that correspond to cloud patchiness, even if the light curve shows no variability.

In addition to photometric and spectroscopic studies, brown dwarfs in our candidate sample can also be studied through polarimetry to detect clouds or hazes in their atmosphere if they show flat light-curves. Luhman 16 is one of the few accessible targets with polarimetry due to its brightness and distance to Earth. Millar-Blanchaer et al. (2020) took *H*-band Very Large Telescope/NaCo linear polarization measurements of the nearby Luhman 16 binary system, and they found that Luhman 16A shows longitudinal cloud bands. Luhman 16A has shown only mild signs of variability in *iz* bands through photometric monitoring (Biller et al. 2013) and in *HST*/WFC3 G102, which covers the peak in the *Y* band (Buenzli et al. 2015a), although no variability has been detected in longer wavelengths. However, polarimetric measurements from Millar-Blanchaer et al. (2020) suggests cloud morphology of banded structures in the NIR. This suggests that the symmetric, banded structure and spin axis inclination of Luhman 16A compound to produce variability amplitudes close to zero (Buenzli et al. 2015b) in the NIR, but we can recover the signature of a blended-light atmosphere (e.g., from different temperature bands) with our empirical technique.

Vos et al. (2017) studied a sample of known *Spitzer Space Telescope* [3.6] and *J*-band variable brown dwarfs, computing the inclination angles of 19 variable brown dwarfs. All objects in the sample with mid-IR variability have an inclination angle greater than 20° , and objects with *J*-band variability have an inclination angle greater than 35° . Vos et al. (2017) determined that *J*-band observations could be more affected by inclination, as they probe deeper into the atmosphere. Their study shows that there is a correlation between inclination and variability detection, and even if a brown dwarf does not show variability, this may be due to inclination effects (Vos et al. 2017): if observed pole-on ($i = 0^\circ$), there will be less rotational variations than if observed equator-on ($i = 90^\circ$). However, since pole-on orientations are significantly less probable than equator-on (Jackson & Jeffries 2010), it is unlikely that most of our variability candidates with future flat light curves would be oriented pole-on. Understanding whether the variability indices technique has a dependence on inclination will be an important step in validating and assessing the technique in future work.

5. CONCLUSIONS

In this paper, we have designed a technique to predict cloud-driven variability in L/T transition brown dwarf atmospheres by studying archival, single-epoch, low-resolution, near-infrared SpeX spectra. We applied the spectral binary indices from

Bardalez Gagliuffi et al. (2014) to a sample of 270 L7–T3 brown dwarfs with SpeX prism spectra available in the SPL, originally used to highlight differences between unresolved binary systems and single source spectra, in order to identify whether certain indices pinpointed peculiarities in the spectrum caused by variability. We identified regions of the index-index plots where benchmark variables were highly concentrated while minimizing the number of non-variable contaminants. We selected the sources that were repeatedly found in multiple regions of variability and chose them as our candidates for variability study. The candidates found in 10 or 11 of the 11 regions are considered variable candidates, and we recommend them for photometric monitoring follow-up. Our conclusions are as follows:

1. We propose a technique to pre-select photometrically variable L7-T3 dwarfs for future monitoring campaigns. Currently there is no method to pre-select which brown dwarfs have higher chances of being variable for monitoring studies. Using this technique can significantly save future resources in next generation telescopes when detecting variability in brown dwarfs.
2. We have identified 62 variability candidates from our sample of 325 L7–T3 integrated light, NIR SpeX spectra following this technique, out of which 50 are entirely new discoveries.
3. Most of our variability candidates have had peculiar spectra or red colors reported in the literature since their discovery and we suggest that their peculiarities are due to variability. Out of our 62 candidates, 14 are confirmed young or show kinematic signatures suggestive of youth. Since variability is more prominent among young sources (Vos et al. 2017), our technique might be biased to identify young variable sources.
4. We are conducting a ground-based NIR survey to further verify our method to find brown dwarf variables. In a future paper we will demonstrate the efficiency of our novel method.
5. Flat light curves of our variability candidates might indicate symmetric surface features such as zonal banding or pole-on inclinations.
6. Based on preliminary photometric monitoring follow up with *Spitzer*, we expect that $\sim 67\%$ of our candidates will show a significant variability amplitude.

We have conducted a spectroscopic analysis of photometric variability, finding 62 unique L7–T3 dwarf candidates for variability from their peculiar spectra. If we can indeed identify variability from single-epoch spectra, we can further investigate spectral characteristics of variable brown dwarfs. This will provide further insight into the chemistry of brown dwarf atmospheres and cloud-formation mechanisms.

D.B.G and A.A. acknowledge funding support from the Astrophysics Data Analysis Program of the National Aeronautics and Space Administration under Grant No. 80NSSC19K0532. This research has made heavy use of the VizieR catalogue access tool and SIMBAD database, operated at CDS, Strasbourg, France. The original description of the VizieR service was published in [Ochsenbein et al. \(2000\)](#), and the SIMBAD astronomical database was published in [Wenger et al. \(2000\)](#). This publication makes use of data from the SpeX Prism Spectral Libraries, maintained by Adam Burgasser at <http://www.browndwarfs.org/spexprism>. We would also like to thank the anonymous reviewer for their careful and thorough comments on our manuscript and their insightful suggestions, which significantly improved our draft. The authors wish to recognize and acknowledge the very significant cultural role and reverence that the summit of Mauna Kea has always had within the indigenous Hawaiian community. We are most fortunate to have the opportunity to conduct observations from this mountain.

Facilities: IRTF(SpeX)

Software: SPLAT ([Burgasser & Splat Development Team 2017](#))

APPENDIX

A. SUMMARY OF SELECTION REGIONS FOR THE FULL SAMPLE

Table A.1. Region limits for each index-index correlation plot.

Name	SpeX SpT	Youth	(1)	(2)	(3)	(4)	(5)	(6)	(7)	(8)	(9)	(10)	(11)	Total
WISE J000622.67-131955.2	L8	0	0	0	1	1	0	0	0	0	0	0	0	2
WISE J00062785+1857288	L7	0	0	0	0	0	0	0	1	0	0	1	1	3
2MASS J00132229-1143006	T3	0	0	0	0	0	0	0	0	0	0	0	0	0
2MASS J00133470+1109403	L7	0	0	0	1	1	0	0	1	0	0	1	1	5
2MASS J00150206+2959323	L8	0	0	0	0	0	0	0	0	0	0	0	0	0
PSO J004.1834+23.0741	T0	0	1	1	1	1	1	1	1	1	1	1	1	11
WISE J00164397+2304265	T1	0	1	1	1	1	1	1	1	1	1	1	1	11
PSO J004.7148+51.8918	L7	0	1	1	1	1	0	1	1	1	0	1	1	9
2MASS J0028394+150141	L7	0	1	1	1	1	1	1	1	1	1	1	1	10
2MASSW J0030300-145033	L7	1	0	0	1	0	0	1	1	0	0	1	1	5
WISE J003110.04+574936.3	L9	0	1	1	1	1	1	1	1	1	1	1	1	11
WISE J003110.04+574936.3	T0	0	1	1	1	1	1	1	1	1	1	1	1	11
SDSSp J003259.36+141036.6	L9	0	1	0	1	1	1	1	1	1	1	1	1	10
SDSSp J003259.36+141036.6	L9	0	0	0	1	1	1	1	1	1	1	1	1	9
2MASS J00440332+0228112	L7	0	1	1	1	1	0	0	1	1	0	1	1	8
WISE J00440339+0228106	L7	0	1	1	1	1	0	0	1	0	0	1	1	7
2MASS J00452972+4237438	L8	0	0	0	0	0	0	0	1	0	0	1	1	3
WISEP J004701.06+680352.1	L7	1	1	1	1	1	1	1	1	1	1	1	1	11
WISE J004928.48+044059.9	L9	0	0	0	1	1	1	1	1	0	1	1	1	8
WISEA J010202.11+035541.4	T0	0	1	1	1	1	1	1	1	1	1	1	1	11
2MASS J0103320+193536	L7	1	1	1	0	0	1	1	1	0	1	1	1	8
2MASS J0103320+193536	L7	0	1	1	1	1	0	0	1	0	0	1	1	7
SDSSp J010752.33+004156.1	L7	1	1	1	1	1	1	1	1	1	1	1	1	11
SDSSp J010752.33+004156.1	L7	0	1	1	1	1	1	1	1	1	1	1	1	11
SDSSp J010752.33+004156.1	L7	0	1	1	1	1	1	1	1	1	1	1	1	11
SDSS J011912.22+240331.6	T2	0	1	1	1	1	1	1	0	1	1	0	0	8

Table A.1 continued on next page

Table A.1 (continued)

Name	SpeX SpT	Youth	(1)	(2)	(3)	(4)	(5)	(6)	(7)	(8)	(9)	(10)	(11)	Total
2MASS J01262109+1428057	L7	1	1	1	0	0	0	1	1	0	0	1	1	6
2MASS J01303563-4445411B	L8	0	1	1	1	1	0	0	1	1	1	1	1	9
PSO J023.8557+02.0884	L8	0	1	1	0	0	1	1	1	1	1	1	1	9
SIMP J013656.57+093347.3	T2	0	1	1	1	1	1	1	1	1	1	1	1	11
WISE J013836.58-032221.2	T3	0	0	0	0	0	0	0	0	0	0	0	0	0
2MASS J01453520-0314117	L9	0	0	0	1	1	0	0	1	0	0	1	1	5
WISE J01453523-0314129	L9	0	0	0	1	1	1	1	1	0	1	1	1	8
WISE J015010.89+382724.1	L9	0	0	0	1	1	1	1	1	0	1	1	1	8
WISE J015010.89+382724.1	L9	0	0	0	1	1	1	0	1	0	1	1	1	7
SDSS J015141.69+124429.6	L9	0	0	0	1	1	1	1	1	0	1	0	1	7
WISE J02022929+2305139	L7	0	1	1	1	1	1	1	1	0	1	1	1	10
DENIS-P J0205.4-1159	L9	0	0	0	1	1	1	0	1	0	1	1	1	7
WISE J020625.27+264023.6	L8	0	1	1	1	1	1	1	1	1	1	1	1	11
WISE J02260916-1610004	L7	0	1	1	1	1	0	1	1	0	0	1	1	8
WISE J023038.90-022554.0	L9	0	1	1	1	1	1	1	1	1	1	1	1	11
SDSSp J023617.93+004855.0	L9	0	0	0	1	1	0	0	1	0	0	1	1	5
SDSS J024749.90-163112.6	T2	0	0	0	0	0	0	0	0	0	0	0	0	0
DENIS-P J0255-4700	L9	0	1	0	1	1	1	1	1	1	1	1	1	10
2MASS J02572581-3105523	L8	0	0	0	1	1	1	1	1	1	1	1	1	9
2MASSW J0306268+154514	L7	0	1	1	1	1	0	1	1	1	0	1	1	9
2MASSW J0310599+164816	T0	0	1	1	1	1	1	1	1	1	1	1	1	11
SIMP J03162759+2650277	T3	0	0	0	0	0	0	0	0	0	0	0	0	0
2MASS J03185403-3421292	L8	1	1	1	1	1	1	1	1	1	1	1	1	11
WISE J032301.86+562558.0	L7	0	1	1	1	1	1	1	1	1	1	1	1	11
2MASS J03231004-4631263	L7	1	0	0	0	0	0	1	0	0	0	0	0	1
WISE J03244023-1919056	L8	0	0	0	0	0	0	0	1	0	1	1	1	4
2MASS J03264225-2102057	L7	1	1	1	1	1	1	1	1	1	1	1	1	11
2MASS J0328426+230205	T0	0	0	1	1	1	1	1	1	1	1	1	1	10
2MASS J03432548+3155165	L7	1	1	1	0	0	0	0	1	0	0	1	1	5

Table A.1 continued on next page

Table A.1 (continued)

Name	SpeX SpT	Youth	(1)	(2)	(3)	(4)	(5)	(6)	(7)	(8)	(9)	(10)	(11)	Total
2MASS J03435056+3203180	L7	1	0	1	0	0	0	0	0	0	0	0	0	1
2MASS J03435721+3201337	L7	1	1	1	0	0	0	0	1	0	0	1	1	5
CI* IC 348 LRL 30003	L7	1	0	0	0	0	0	0	0	0	0	0	0	0
CI* IC 348 LRL 1923	L7	1	0	0	0	0	0	0	0	0	0	0	0	0
2MASS J03440291+3152277	L8	1	0	0	0	0	0	0	1	0	0	1	1	3
CI* IC 348 LRL 1925	L7	1	1	1	0	0	0	0	1	1	0	1	1	6
2MASS J03441150+3218094	L8	1	0	0	1	1	0	0	1	0	0	1	1	5
2MASS J03441386+3156539	L7	1	1	1	0	0	0	0	1	0	0	1	1	5
[PSZ2003] J034426.5+320820	L7	1	0	0	0	0	0	0	1	0	0	1	1	3
[PSZ2003] J034427.2+320346	L8	1	0	0	1	1	0	0	1	0	0	1	1	5
2MASS J03443687+3214363	L7	1	0	0	0	0	0	0	1	0	0	1	1	3
CI* IC 348 MM 74	L7	1	0	0	0	0	0	0	1	0	0	1	1	3
[PSZ2003]J034444.9+321411	L7	1	0	0	0	0	0	0	1	0	0	1	1	3
2MASS J03444520+3201197	L7	1	1	1	0	0	0	0	1	1	0	1	1	6
2MASS J03445853+3158270	L7	1	0	0	0	0	0	0	1	0	0	1	1	3
2MASS J03450644+3159394	L7	1	0	0	0	0	0	0	1	0	0	1	1	3
2MASS J03451604+3205140	L7	1	0	0	0	0	0	0	0	0	0	0	0	0
2MASS J03452212+3205450	L7	1	0	0	0	0	0	0	1	0	0	1	1	3
IC 348 IRS J03452901+3217551	L8	1	0	0	1	0	0	0	1	0	0	1	1	4
PSO J057.2893+15.2433	L7	0	1	1	0	0	0	1	1	1	0	1	1	7
SDSS J035104.37+481046.8	T2	0	0	0	0	0	0	0	0	0	0	0	0	0
2MASS J03552337+1133437	L7	1	1	1	0	0	0	1	1	1	0	1	1	7
2MASS J03582213-4116144	L7	1	1	1	1	1	0	0	1	0	1	1	1	8
2MASS J04144158+2809583	L7	1	0	0	0	0	0	0	1	0	0	1	1	3
V410 Anon 13	L7	1	0	0	0	0	0	0	1	0	0	1	1	3
IRAS F04262+2654	L7	1	0	0	0	0	0	1	1	0	0	1	1	4
2MASS J04325026+2422115	L7	1	1	1	0	0	0	0	1	0	0	1	1	5
CFHT 1	L7	1	0	0	0	0	0	0	1	0	0	1	1	3
2MASS J0435145-141446	L7	1	0	0	0	0	0	1	1	0	0	1	1	4

Table A.1 continued on next page

Table A.1 (continued)

Name	SpeX SpT	Youth	(1)	(2)	(3)	(4)	(5)	(6)	(7)	(8)	(9)	(10)	(11)	Total
2MASS J04354290+1323449	L7	0	0	0	0	0	1	0	0	0	1	0	0	2
2MASS J04373705+2331080	L7	0	0	0	0	0	0	0	1	0	0	1	1	3
2MASS J04381486+2611399	L7	1	0	0	0	0	0	0	1	0	0	1	1	3
CFHT 4	L8	1	0	0	0	0	0	0	1	0	0	1	1	3
WISE J044633.45-242956.9	T0	0	0	0	1	0	0	0	1	0	0	1	1	4
PSO J071.8769-12.2713	T1	0	0	0	0	0	0	0	0	0	0	0	0	0
WISE J045746.08-020719.2	T2	0	0	0	0	0	0	1	0	0	0	0	0	1
2MASS J05012406-0010452	L7	1	1	1	1	1	0	1	1	0	0	1	1	8
2MASS J05185995-2828372	T2	0	0	0	0	0	0	0	0	0	0	0	0	0
WISE J060738.65+242953.5	L9	0	0	0	1	1	0	1	1	0	0	1	1	6
WISE J060738.65+242953.5	L9	0	0	0	1	1	1	1	1	0	1	1	1	8
WISE J061135.13-041024.0	T0	0	1	1	1	1	0	0	1	0	1	1	1	8
2MASS J06244595-4521548	L7	1	0	0	1	1	0	0	0	0	0	0	0	2
WISE J062905.13+241804.9	T0	0	0	0	0	0	0	0	0	0	0	0	0	0
2MASS J06420559+4101599	L8	0	1	1	1	1	1	1	1	1	1	1	1	11
PSO J103.0927+41.4601	T0	0	1	1	1	1	1	1	1	1	1	1	1	11
WISE J065609.59+420531.9	T3	0	0	0	0	0	0	0	0	0	0	1	0	1
WISE J07053400-1839256	L8	0	0	0	1	0	0	0	1	0	0	1	1	4
SDSS J073922.26+661503.5	T2	0	1	1	1	0	1	1	1	1	1	1	1	10
SDSS J073922.26+661503.5	T1	0	0	0	0	0	1	1	0	0	1	0	0	3
2MASS J0756252+124456	T0	0	1	1	1	1	0	0	0	1	1	0	0	6
SDSS J075840.33+324723.4	T2	0	1	1	1	1	1	1	1	1	1	1	1	11
SDSS J080531.84+481233.0	L7	0	0	0	0	1	0	0	0	0	0	0	0	1
SDSS J080531.84+481233.0	T0	0	0	0	1	1	0	0	0	0	0	0	0	2
WISE J080700.23+413026.8	L8	0	0	0	1	1	0	0	1	0	0	1	1	5
SDSS J080959.01+443422.2	L7	0	1	1	1	1	1	1	1	1	1	1	1	11
SDSS J080959.01+443422.2	L7	0	1	1	1	1	0	1	1	1	1	1	1	10
SDSS J082030.12+103737.0	T0	0	1	1	1	1	1	1	1	1	1	1	1	11
SDSS J082030.12+103737.0	T0	0	0	1	1	1	1	1	1	1	1	1	1	10

Table A.1 continued on next page

Table A.1 (continued)

Name	SpeX SpT	Youth	(1)	(2)	(3)	(4)	(5)	(6)	(7)	(8)	(9)	(10)	(11)	Total
2MASS J0825196+211552	L8	1	1	1	1	1	1	1	1	1	1	1	1	11
2MASS J0829570+265510	L7	0	1	1	1	1	1	1	1	1	1	1	1	11
SDSSp J083008.12+482847.4	T0	0	1	1	1	1	1	1	1	1	1	1	1	11
SDSSp J083008.12+482847.4	T0	0	1	1	1	1	1	1	1	1	1	1	1	11
2MASS J0835425-081923	L7	0	0	0	1	1	1	0	0	0	1	0	0	4
SDSSp J083717.22-000018.3	T1	0	1	1	1	1	1	1	1	1	1	1	1	11
SDSSp J083717.22-000018.3	T1	0	1	1	1	1	1	1	1	1	1	1	1	11
SDSSp J083717.22-000018.3	T1	0	1	1	1	1	1	1	1	1	1	0	1	10
2MASSs J0850359+105716	L7	0	1	1	1	1	1	1	1	1	1	1	1	11
2MASSs J0850359+105716	L7	0	1	1	1	1	1	1	1	1	1	1	1	11
SDSS J085234.90+472035.0	T0	0	1	1	1	1	1	1	1	1	1	1	1	11
SDSSp J085758.45+570851.4	L8	0	1	1	1	1	1	1	1	1	1	1	1	11
SDSS J085834.42+325627.7	T0	0	1	1	1	1	1	0	1	1	1	1	1	10
SDSS J085834.42+325627.7	T0	0	1	1	1	1	1	0	0	1	1	0	0	7
2MASS J0859254-194926	L7	0	1	1	1	1	1	1	1	1	1	1	1	11
2MASS J0859254-194926	L8	0	0	0	1	1	1	1	1	1	1	1	1	9
2MASS J0859254-194926	L8	0	0	0	1	1	1	1	1	1	1	1	1	9
SDSS J090900.73+652527.2	T1	0	0	0	0	0	0	0	1	0	0	1	1	3
GI 337CD	L9	0	0	0	0	0	0	1	1	0	0	0	1	3
GI 337CD	T0	0	0	0	1	0	0	1	1	0	0	1	1	5
2MASS J09175418+6028065	L7	1	1	1	1	1	1	1	0	0	1	0	0	7
2MASS J0920122+351742	L9	0	0	0	1	1	1	1	1	1	1	1	1	9
WISE J092055.40+453856.3	T0	0	1	1	0	0	1	1	1	1	1	1	1	9
2MASS J0929336+342952	L8	0	1	1	1	1	1	1	1	1	1	1	1	11
SDSS J093109.56+032732.5	T0	0	1	1	1	1	1	1	1	1	1	1	1	11
2MASS J09490860-1545485	T2	0	0	0	0	0	0	0	0	0	0	0	0	0
2MASS J09490860-1545485	T2	0	0	0	0	0	0	0	0	0	0	0	0	0
LP 261-75B	L7	0	0	0	1	0	0	0	1	0	0	1	1	4
2MASS J09553336-0208403	L8	0	1	1	1	1	1	1	1	1	1	1	1	11

Table A.1 continued on next page

Table A.1 (continued)

Name	SpeX SpT	Youth	(1)	(2)	(3)	(4)	(5)	(6)	(7)	(8)	(9)	(10)	(11)	Total
SIMP J09560810-1447065	T0	0	1	1	1	1	1	1	1	1	1	1	1	11
PSO J149.1907-19.1730	T0	0	0	0	1	1	0	0	0	0	0	0	0	2
2MASS J10020752+1358556	L7	0	0	1	0	1	0	0	0	0	0	0	0	2
G 196-3B	L7	1	1	1	1	1	0	0	1	0	0	1	1	7
G 196-3B	L7	0	1	1	1	1	0	0	1	0	0	1	1	7
SDSS J100711.74+193056.2	T0	0	1	1	1	1	1	1	1	1	1	1	1	11
SDSS J100711.74+193056.2	L9	0	1	1	1	1	1	1	1	1	1	1	1	11
SDSS J102109.69-030420.1	T3	0	0	0	0	0	0	0	0	0	0	0	0	0
SDSS J102552.43+321234.0	L8	0	0	0	1	1	0	1	1	1	1	1	1	8
SDSS J102552.43+321234.0	L8	0	1	0	1	0	1	0	1	1	0	1	0	6
2MASS J10293958+5715445	L9	0	0	0	1	1	1	1	1	0	1	1	1	8
SDSS J103026.78+021306.4	L9	0	0	0	1	1	1	1	1	0	1	1	1	8
SDSS J103321.92+400549.5	L7	0	0	0	1	1	1	1	1	0	0	1	1	7
2MASSW J1036530-344138	L9	0	0	0	1	1	0	1	1	0	0	1	1	6
SDSS J103931.35+325625.5	T2	0	0	1	1	1	0	0	0	0	1	0	0	4
SDSS J103931.35+325625.5	T2	0	1	1	1	1	1	0	0	1	1	0	0	7
2MASS J10430758+2225236	T0	0	1	1	1	1	1	1	1	1	1	1	1	11
SDSS J104335.08+121314.1	L9	0	1	1	1	1	1	1	1	1	1	1	1	11
SDSS J104335.08+121314.1	L9	0	1	1	1	1	1	1	1	1	1	1	1	11
SDSS J104409.43+042937.6	L8	0	0	0	1	1	1	1	1	0	1	1	1	8
SDSS J104829.21+091937.8	T2	0	0	0	0	0	0	1	0	0	0	0	0	1
WISE J104915.57-531906.1A	L9	0	1	1	1	1	1	1	1	1	1	1	1	11
WISE J104915.57-531906.1B	T1	0	1	1	1	1	1	1	1	1	1	1	1	11
SDSS J105213.51+442255.7	T0	0	1	1	1	1	1	1	1	1	1	1	1	11
2MASS J11061191+2754215	T2	0	0	0	0	0	0	0	0	0	0	0	0	0
2MASS J11181292-0856106	L9	0	0	0	1	1	1	1	0	0	1	0	0	4
2MASS J11181292-0856106	L9	0	0	0	1	1	1	1	0	1	0	1	1	7
2MASS J11193254-1137466	L7	0	1	1	1	1	1	1	1	1	1	1	1	11
SDSS J112118.57+433246.5	T0	0	0	0	1	1	1	1	1	1	1	1	1	9

Table A.1 continued on next page

Table A.1 (continued)

Name	SpeX SpT	Youth	(1)	(2)	(3)	(4)	(5)	(6)	(7)	(8)	(9)	(10)	(11)	Total
2MASS J11220826-3512363	T2	0	0	0	0	0	0	0	0	0	0	0	0	0
2MASS J11472421-2040204	L7	0	1	1	1	1	1	1	1	1	1	1	1	11
SDSS J115553.86+055957.5	L9	0	0	0	1	1	1	1	1	1	1	1	1	9
WISE J120035.40-283657.5	T0	0	0	0	1	1	1	1	1	0	1	1	1	8
WISE J120035.40-283657.5	L9	0	0	0	1	1	1	1	1	0	1	1	1	8
WISE J12010457+5730042	T0	0	1	1	1	1	1	1	1	1	1	1	1	11
SDSS J120602.51+281328.7	T3	0	0	0	0	0	0	0	0	0	0	0	0	0
SDSS J120747.17+024424.8	T0	0	0	0	1	1	0	0	1	0	0	1	1	5
2MASS J12095613-1004008	T3	0	0	0	0	0	0	0	0	0	0	0	0	0
2MASS J12095613-1004008	T3	0	0	0	0	0	0	0	0	0	0	0	0	0
SDSS J121951.45+312849.4	T0	0	1	1	1	1	1	1	1	1	1	1	1	11
2MASS J12304602+2827515	L7	0	0	0	0	0	0	0	0	0	0	0	0	0
SDSSp J125453.90-012247.4	T2	0	1	1	1	1	1	1	1	1	1	1	1	11
2MASS J13043568+1542521	T0	0	0	0	0	0	0	0	0	0	0	0	0	0
WISE J13052306-3951049	L8	0	1	1	0	1	0	0	0	1	1	0	0	5
2MASS J13064517+4548552	L9	0	0	0	1	1	1	1	0	1	0	1	0	6
WISEA J130729.56-055815.4	L8	0	0	0	1	0	0	0	1	0	0	1	1	4
PSO J201.0320+19.1072	T3	0	0	0	0	0	0	0	0	0	0	0	0	0
2MASS J13243553+6358281	T3	0	1	1	1	1	1	1	1	1	1	1	1	11
2MASSW J1326201-272937	L7	0	1	1	1	1	1	1	1	1	1	1	1	11
SDSSp J132629.82-003831.5	L7	0	1	1	1	1	0	1	1	1	1	1	1	10
SDSS J133148.92-011651.4	T0	0	1	1	1	1	1	1	1	1	1	1	1	11
SDSS J133148.92-011651.4	T0	0	1	1	1	1	1	1	1	1	1	1	1	11
SDSS J133148.92-011651.4	T0	0	1	1	1	1	1	1	1	1	1	1	1	11
WISE J134310.44-121628.8	T0	0	0	0	1	1	1	1	1	0	1	1	1	8
SIMP J13441371-1614022	T0	0	0	0	1	1	0	0	0	0	0	0	0	2
WISE J134806.99+660328.4	L8	0	1	1	0	0	1	1	1	1	1	1	1	9
SDSS J140023.12+433822.3	L8	0	0	0	1	0	0	1	1	0	0	1	1	5
WISE J140035.40-385013.5	T3	0	0	0	0	0	0	0	0	0	0	0	0	0

Table A.1 continued on next page

Table A.1 (continued)

Name	SpeX SpT	Youth	(1)	(2)	(3)	(4)	(5)	(6)	(7)	(8)	(9)	(10)	(11)	Total
2MASS J14025564+0800553	T0	0	1	1	0	0	0	0	0	0	1	0	0	3
2MASS J14044948-3159330	T2	0	0	0	0	0	0	0	0	0	0	0	0	0
2MASS J14111847+2948515	T0	0	0	0	1	1	1	0	0	0	0	1	0	4
SDSS J141530.05+572428.7	T3	0	0	0	0	0	0	0	0	0	0	0	0	0
SDSS J141659.78+500626.4	L7	0	0	0	1	1	1	1	0	1	0	1	1	7
WISE J14321117+3244338	L7	0	0	0	1	1	1	1	1	0	1	1	1	8
SDSS J143553.25+112948.6	T2	0	0	0	0	0	0	0	0	0	0	0	0	0
SDSS J143945.86+304220.6	T2	0	0	0	0	0	0	0	0	0	0	0	0	0
WISE J150406.66-455223.9	L8	0	0	0	1	1	1	0	1	0	0	1	1	5
PSO J226-2599-28.8959	T1	0	0	0	0	0	1	0	1	0	1	1	1	5
SDSS J151114.66+060742.9	L9	0	0	0	1	0	0	0	0	0	0	0	0	1
SDSS J151114.66+060742.9	T0	0	1	0	0	0	0	0	0	0	0	0	0	1
WISE J151314.61+401935.6	L9	0	1	1	1	1	1	1	1	1	1	1	1	11
SDSS J151506.11+443648.3	L7	0	1	1	1	1	1	1	1	1	1	1	1	11
SDSS J151603.03+025928.9	T0	0	0	1	1	1	0	0	0	0	0	0	0	3
SDSS J151643.01+305344.4	T2	0	1	1	1	1	1	1	1	1	1	1	1	11
SDSS J152039.82+354619.8	T0	0	0	0	0	0	1	1	1	0	1	1	1	6
SDSS J152039.82+354619.8	L9	0	0	0	1	1	1	1	1	1	1	1	1	9
SDSS J152103.24+013142.7	T2	0	0	0	0	0	0	0	0	0	0	0	0	0
Gliese 584C	L8	0	0	1	1	1	0	1	1	1	1	1	1	9
WISE J15335852+4757069	L7	0	1	1	0	0	1	1	1	1	1	1	1	9
SDSS J153417.05+161546.1AB	T3	0	0	0	0	0	0	0	0	0	0	0	0	0
SDSS J154009.36+374230.3	L9	0	1	1	1	1	1	1	1	1	1	1	1	11
SDSS J154009.36+374230.3	L9	0	1	1	1	1	1	1	1	1	1	1	1	11
2MASS J15423630-0045452	T0	0	0	0	1	1	1	1	1	0	1	1	1	8
SDSS J154508.93+355527.3	L8	0	0	0	0	0	0	0	1	0	0	1	1	3
2MASS J15461461+4932114	T2	0	0	0	0	0	0	0	0	0	0	0	0	0
2MASS J15461461+4932114	T2	0	0	0	0	0	0	0	0	0	0	0	0	0
SDSS J154849.02+172235.4	L8	0	0	0	1	1	1	1	0	1	1	1	1	8

Table A.1 continued on next page

Table A.1 (continued)

Name	SpeX SpT	Youth	(1)	(2)	(3)	(4)	(5)	(6)	(7)	(8)	(9)	(10)	(11)	Total
2MASS J15515237+0941148	L7	1	0	0	0	1	0	0	0	0	0	1	1	3
2MASS J15515237+0941148	L7	0	1	1	1	1	0	0	1	0	0	1	1	7
WISE J155254.84+503307.6	L9	0	0	1	1	1	0	0	0	0	0	0	0	3
2MASSW J1553214+210907	L7	0	1	1	0	0	1	1	1	0	1	1	1	8
2MASS J16154255+4953211	L7	1	1	1	0	0	0	1	1	1	0	1	1	7
2MASS J16154255+4953211	L7	0	1	1	1	1	0	1	1	1	0	1	1	9
2MASS J16154255+4953211	L7	0	1	1	1	1	0	1	1	1	0	1	1	9
PSO J244.1180+06.3598	L7	0	1	1	1	1	1	1	0	1	1	1	1	10
PSO J247.3273+03.5932	T2	0	1	1	1	1	1	1	1	1	1	1	1	11
SDSS J163030.53+434404.0	L9	0	1	1	1	1	1	1	1	1	1	1	1	11
2MASSW J1632291+190441	L8	0	1	1	1	1	1	1	1	1	1	1	1	11
2MASSW J1632291+190441	T0	0	0	1	1	1	1	1	1	1	1	1	1	10
SDSS J163239.34+415004.3	T1	0	0	0	0	0	1	1	0	0	1	0	0	3
WISE J164715.57+563208.3	L8	0	1	1	1	1	1	1	1	1	1	1	1	11
2MASS J17021901-2235022	L7	0	0	0	0	0	0	1	1	0	0	0	1	3
2MASS J1711457+223204	T0	0	1	1	1	1	0	0	0	1	0	0	0	5
2MASS J1721039+334415	T0	0	0	0	1	1	1	1	1	0	1	1	1	8
WISEA J172120.69+464025.9	T0	0	0	0	1	1	1	0	1	0	1	1	1	7
2MASSW J1728114+394859	L7	0	1	1	1	1	0	1	1	1	0	1	1	9
2MASSW J1728114+394859	L7	0	0	1	1	1	0	1	1	1	1	1	1	9
WISE J173035.99+420742.1	T0	0	0	0	0	0	0	0	0	0	0	0	0	0
SDSS J173101.41+531047.9	L7	0	0	1	1	1	1	0	0	0	1	0	0	5
2MASS J17373467+5953434	L9	0	0	0	1	1	0	0	0	0	0	0	0	2
WISE J173859.27+614242.1	L7	0	1	1	1	1	1	1	1	1	1	1	1	11
2MASS J17392515+2454421	L7	0	0	0	1	1	1	0	1	0	1	1	1	7
WISE J17405782+1317094	L9	0	0	0	1	1	0	0	1	0	0	1	1	5
WISE J174102.78-464225.5	L7	1	1	1	1	1	1	1	1	1	1	1	1	11
SDSS J175024.01+422237.8	T2	0	1	1	0	1	1	1	1	1	1	1	1	10
SDSSp J175032.96+175903.9	T3	0	0	0	0	0	0	0	0	0	0	0	0	0

Table A.1 continued on next page

Table A.1 (continued)

Name	SpeX SpT	Youth	(1)	(2)	(3)	(4)	(5)	(6)	(7)	(8)	(9)	(10)	(11)	Total
WISE J175510.28+180320.2	T1	0	0	0	1	0	1	1	0	0	0	0	0	3
WISEP J180026.60+013453.1	L8	0	0	0	1	1	1	1	1	1	1	1	1	9
WISE J180952.53-044812.5	T0	0	0	0	1	1	1	1	1	0	1	1	1	8
WISE J180952.53-044812.5	T0	0	0	0	1	1	1	1	1	0	1	1	1	8
WISE J180952.53-044812.5	T1	0	0	0	1	1	1	1	1	0	1	1	1	8
WISE J183058.56+454257.4	L9	0	1	1	1	1	1	1	1	1	1	1	1	11
WISE J185101.83+593508.6	L9	0	1	1	1	1	1	1	1	1	1	1	1	11
WISE J185101.83+593508.6	L9	0	0	0	1	1	1	0	1	0	1	1	1	7
DENIS J19013910-3700170	L7	1	0	0	0	0	0	1	1	0	0	1	1	4
WISE J191915.54+304558.4	L7	0	0	0	1	1	0	1	1	0	0	1	1	6
2MASS J20025073-0521524	L7	1	1	1	1	1	1	0	1	1	1	1	1	10
2MASS J20025073-0521524	L7	0	1	1	1	1	1	1	1	1	1	1	1	11
2MASS J20025073-0521524	L7	0	1	1	1	1	1	1	1	1	1	1	1	11
WISE J201204.10+672607.9	L7	0	0	0	0	0	1	0	0	0	1	0	0	2
WISE J203042.79+074934.7	T1	0	0	0	0	0	1	1	1	0	1	1	1	6
WISE J203042.79+074934.7	T1	0	0	0	1	0	1	1	1	0	1	1	1	7
SDSS J204317.69-155103.4	L9	0	0	0	0	1	1	1	1	0	1	1	1	7
SDSS J204317.69-155103.4	L9	0	0	0	0	0	1	1	1	0	1	0	1	5
SDSS J204317.69-155103.4	L9	0	0	0	1	1	1	1	1	1	1	0	1	8
WISE J204356.42+622049.0	T1	0	0	0	1	1	1	1	1	1	1	1	1	9
SDSS J204749.61-071818.3	L9	0	0	0	1	1	1	1	1	0	1	1	1	8
WISEA J205202.06-204313.0	L8	0	0	0	0	0	0	0	1	0	0	1	1	3
SDSS J205235.31-160929.8	T0	0	0	0	1	1	0	0	1	0	0	0	1	4
SDSS J205235.31-160929.8	T0	0	0	0	1	0	0	1	1	0	0	0	1	4
SDSS J205235.31-160929.8	T1	0	0	0	1	1	0	0	1	0	1	1	1	6
2MASSW J2101154+175658	L9	0	1	1	1	1	1	1	1	1	1	1	1	11
2MASSW J2101154+175658	L7	0	0	0	1	1	0	0	1	0	0	1	1	5
2MASSW J2101154+175658	L8	0	1	1	1	1	1	1	1	1	1	1	1	11
PSO J319.3102-29.6682	T0	0	0	0	1	0	1	1	1	0	1	1	1	7

Table A.1 continued on next page

Table A.1 (continued)

Name	SpeX SpT	Youth	(1)	(2)	(3)	(4)	(5)	(6)	(7)	(8)	(9)	(10)	(11)	Total
2MASS J21243864+1849263	T0	0	1	1	1	1	1	1	1	1	1	1	1	11
SDSS J213154.43-011939.3	L9	0	1	1	1	1	1	1	1	1	1	1	1	11
2MASS J21321145+1341584	L7	0	0	0	1	1	0	0	1	0	0	1	1	5
2MASS J21324898-1452544	T3	0	0	0	0	0	0	0	0	0	0	0	0	0
2MASS J21392676+0220226	T2	0	1	1	1	1	1	1	1	1	1	1	1	11
HN Peg B	T3	0	1	1	1	1	1	1	1	1	1	1	1	11
2MASS J21481628+4003593	L7	0	1	1	1	1	1	1	1	1	1	1	1	11
2MASS J21481628+4003593	L7	0	1	1	1	1	1	1	1	1	1	1	1	11
2MASS J21513979+3402444	L8	0	0	0	1	1	0	0	1	0	0	1	1	5
2MASS J21522609+0937575	L7	0	1	1	1	1	1	1	1	0	1	1	1	10
PSO J331.6058+33.0207	T1	0	0	0	1	0	1	1	0	0	1	0	0	4
2MASS J22092183-2711329	T2	0	0	0	0	0	0	0	0	0	0	0	0	0
2MASS J22120703+3430351	L7	0	0	0	0	1	0	0	1	0	0	1	1	4
2MASS J22153705+2110554	T1	0	1	1	1	1	0	1	1	1	1	1	1	10
2MASS J22153705+2110554	T0	0	1	1	1	1	1	1	1	1	1	1	1	11
PSO J334.1193+19.8800	T3	0	0	0	0	0	0	0	0	0	0	0	0	0
WISE J222219.93+302601.4	L8	0	0	0	1	1	1	1	1	1	1	1	1	9
PSO J336.9036-18.9148	L7	0	1	1	0	0	0	0	1	0	0	1	1	5
ULAS J222958.30+010217.2	T3	0	0	0	0	0	0	0	0	0	0	0	0	0
WISEA J223343.53-133140.9	T2	0	0	0	0	0	0	0	0	0	0	0	0	0
WISE J223937.55+161716.1	T3	0	0	0	0	0	0	0	0	0	0	0	0	0
2MASSW J2244316+204343	L7	1	1	1	1	1	1	1	1	1	1	1	1	11
2MASS J22490917+3205489	L7	0	0	0	0	0	0	0	0	0	0	0	0	0
PSO J342.3797-16.4665	T0	0	0	0	0	0	0	0	1	0	0	1	1	3
SDSSp J224953.45+004404.2AB	L7	1	1	1	1	1	0	1	1	0	0	1	1	8
SDSSp J224953.45+004404.2AB	L7	0	0	0	1	1	0	1	1	0	0	1	1	6
BRLT 317	T0	0	0	0	1	1	1	0	1	0	1	1	1	7
DENIS-P J225210.73-173013.4	T0	0	0	0	1	1	0	0	0	0	0	0	0	2
WISEA J230329.45+315022.7	T2	0	0	0	0	0	0	0	0	0	0	0	0	0

Table A.1 continued on next page

Table A.1 (continued)

Name	SpeX SpT	Youth	(1)	(2)	(3)	(4)	(5)	(6)	(7)	(8)	(9)	(10)	(11)	Total
WISEA J230329.45+315022.7	T2	0	0	0	0	0	0	0	0	0	0	0	0	0
PSO J348.8808+06.2873	L7	1	0	0	0	0	0	1	1	0	0	1	1	4
WISE J23230708+0541130	L8	0	0	0	1	1	0	0	1	0	1	1	1	6
2MASS J23254530+4251488	L8	0	0	0	1	1	1	1	1	1	1	1	1	9
WISE J232728.74-273056.6	T0	0	1	1	1	1	1	1	1	1	1	1	1	11
CFBDS J233051-084454	L8	0	0	0	1	1	1	1	1	1	1	1	1	9
2MASS J23322678+1234530	T0	0	1	1	1	1	1	0	0	1	1	0	0	7
2MASS J23352734+4511442	L7	0	1	1	1	1	1	1	1	1	1	1	1	11
WISE J23542231-0811297	L7	0	1	1	1	1	0	1	1	0	0	1	1	8

NOTE—Order of columns (1) H₂O–J vs. CH₄–H, (2) H₂O–J vs. H–bump, (3) CH₄–J vs. CH₄–H, (4) CH₄–J vs. H–bump, (5) CH₄–H vs. H₂O–K, (6) CH₄–H vs. CH₄–K, (7) CH₄–H vs. H–dip, (8) CH₄–H vs. J–curve, (9) H₂O–K vs. H–bump, (10) H–dip vs. K–slope, (11) H–dip vs. H–bump

B. CANDIDATE AND CONFIRMED SPECTRAL BINARIES IN THE SAMPLE

Table A.2. L7–T3 dwarf spectral binary candidates from our index-selection technique.

Source	SpeX SpT	J mag	K mag	Total	SNR	Reference ^a
Confirmed Spectral Binaries						
2MASS J04473039-1216155	T1.0	16.48±0.11	15.55±0.22	5	10.10	3;1;3
2MASS J05185995-2828372	T2.0	15.978±0.1	14.162±0.07	6	56.00	13;13;5
WISE J061135.13-041024.0	T0.0	15.489±0.06	14.221±0.07	3	23.00	20;18;18
SDSS J080531.84+481233.0	L7.0	14.734±0.04	13.444±0.04	3	23.00	12;7;15
GI 337CD	L9.0	15.512±0.08	14.043±0.06	2	84.00	9;1;15
SDSS J102109.69-030420.1	T3.0	16.253±0.09	15.126±0.17	6	31.00	5;18;15
WISE J104915.57-531906.1A	L9.0	11.511±0.03	9.559±0.03	2	133.00	10;10;23
2MASS J11061191+2754215	T2.0	14.879±0.03	13.788±0.04	4	78.00	24;9;30
2MASS J12095613-1004008	T3.0	15.914±0.07	15.062±0.14	4	15.00	11;9;25
2MASS J14044948-3159330	T2.0	15.577±0.06	14.538±0.1	6	33.00	24;18;15
SDSS J153417.05+161546.1AB	T3.0	16.753±0.13	>16.411	5	20.00	12;18;28
SDSS J151114.66+060742.9	L9.0	16.016±0.08	14.544±0.1	6	15.00	12;9;11
SDSS J205235.31-160929.8	T0.0	16.334±0.12	15.123±0.15	2	4.00	12;9;15
DENIS-P J225210.73-173013.4	T0.0	14.313±0.03	12.901±0.02	2	125.00	33;9;33
Confirmed Variable Sources						
SDSS J075840.33+324723.4	T2.0	14.947±0.04	13.879±0.06	2	113.00	8;9; ...
SDSS J085834.42+325627.7	T0.0	16.453±0.12	14.756±0.1	4	20.00	12;1; ...
2MASS J11220826-3512363	T2.0	15.019±0.04	14.383±0.07	2	50.00	5;1; ...
2MASS J13243553+6358281	T3.0	15.596±0.07	14.058±0.06	2	39.00	24;9; ...
2MASS J16291840+0335371	T2.0	15.29±0.04	14.18±0.06	2	75.00	16;1; ...
WISE J180952.53-044812.5	T0.0	15.14±0.05	13.96±0.06	2	56.00	29;1; ...
SDSS J204317.69-155103.4	L9.0	16.625±0.16	15.402±0.21	2	8.00	12;1; ...
HN Peg B	T3.0	15.86±0.03	15.12±0.03	3	55.00	26;1; ...
2MASS J22153705+2110554	T1.0	16.0±0.08	14.82±0.11	2	53.71	32;21; ...
Candidate Spectral Binaries						
WISE J000622.67-131955.2	L8.0	16.67±0.13	15.12±0.13	3	20.00	27;1; ...
WISE J00164397+2304265	T1.0	16.412±0.0	14.973±0.0	2	32.80	3;3; ...
SDSS J011912.22+240331.6	T2.0	17.017±0.18	>17.042	4	24.00	12;9; ...
SDSS J024749.904-163112.6	T2.0	17.186±0.18	15.616±0.19	6	24.00	12;9; ...
SIMP J03162759+2650277	T3.0	16.585±0.15	>15.159	4	33.74	32;3; ...
SDSS J035104.37+481046.8	T2.0	16.466±0.13	14.996±0.12	6	14.00	12;9; ...
WISE J045746.08-020719.2	T2.0	14.897±0.04	14.022±0.06	3	87.00	38;1; ...
WISE J062905.13+241804.9	T0.0	16.34±0.13	15.13±0.15	6	22.00	29;29; ...
PSO J103.0927+41.4601	T0.0	15.48±0.06	13.89±0.05	2	73.00	2;3; ...
SDSS J073922.26+661503.5	T1.0	16.823±0.13	15.831±0.18	2	15.00	12;1; ...
2MASSI J0756252+124456	T0.0	16.659±0.14	14.73±0.12	2	34.00	38;1; ...
SDSSp J083717.22-000018.3	T1.0	17.101±0.21	>15.674	2	10.00	5;1; ...
SDSS J090900.73+652527.2	T1.0	16.034±0.09	15.171±0.15	2	30.00	12;9; ...

Table A.2 continued on next page

Table A.2 (*continued*)

Source	SpeX SpT	J mag	K mag	Total	SNR	Reference ^a
2MASS J09490860–1545485	T2.0	16.149±0.12	15.227±0.17	2	19.00	5;9; ...
2MASS J09564583–1910227	T0.0	15.208±0.05	13.853±0.05	3	47.40	3;3; ...
2MASS J10020752+1358556	L7.0	17.19±0.26	15.59±0.2	4	18.49	21;21; ...
SDSS J103931.35+325625.5	T2.0	16.405±0.15	15.151±0.16	3	15.00	12;9; ...
SDSS J120602.51+281328.7	T3.0	16.541±0.11	>15.817	2	24.00	12;9; ...
SDSS J120747.17+024424.8	T0.0	15.58±0.07	13.986±0.06	2	88.00	24;9; ...
2MASS J12304602+2827515	L7.0	16.073±0.09	14.434±0.06	2	8.00	34;1; ...
2MASS J13043568+1542521	T0.0	17.32±0.19	15.67±0.19	6	41.92	21;21; ...
2MASS J13064517+4548552	L9.0	17.009±0.2	15.499±0.16	2	14.46	22;21; ...
WISE J140035.40–385013.5	T3.0	16.04±0.1	>16.07	2	10.00	29;1; ...
2MASS J14025564+0800553	T0.0	16.85±0.03	15.73±0.03	6	49.17	21;21; ...
2MASS J14111847+2948515	T0.0	16.2±0.09	15.09±0.11	2	29.15	32;1; ...
SDSS J141530.05+572428.7	T3.0	16.734±0.16	>15.544	6	19.00	9;9; ...
SDSS J143553.25+112948.6	T2.0	17.137±0.23	>16.906	5	7.00	12;9; ...
SDSS J143945.86+304220.6	T2.0	17.223±0.23	>15.881	4	22.00	12;9; ...
WISE J150406.66–455223.9	L8.0	16.56±0.11	14.83±0.1	2	14.00	37;1; ...
2MASS J15050230–2853408	T1.0	15.83±0.07	15.06±0.13	2	47.00	14;1; ...
SDSS J151603.03+025928.9	T0.0	17.23±0.2	15.433±0.18	4	29.00	9;9; ...
SDSS J151643.01+305344.4	T2.0	16.848±0.15	15.081±0.09	2	33.00	9;9; ...
2MASS J15461461+4932114	T2.0	15.902±0.07	>14.9	3	16.00	31;1; ...
WISE J155254.84+503307.6	L9.0	17.13±0.24	15.46±0.16	4	12.00	37;1; ...
2MASSI J1711457+223204	T0.0	17.089±0.18	14.727±0.1	6	23.00	9;9; ...
WISEA J172120.69+464025.9	T0.0	16.859±0.15	15.234±0.13	2	15.40	36;1; ...
WISE J173035.99+420742.1	T0.0	16.95±0.18	>15.65	5	35.00	29;1; ...
2MASS J17373467+5953434	L9.0	16.879±0.16	15.719±0.26	2	24.00	19;21; ...
WISE J17405782+1317094	L9.0	>17.468	15.195±0.15	2	19.09	35;1; ...
SDSSp J175032.96+175903.9	T3.0	16.34±0.1	15.478±0.19	2	33.00	11;1; ...
WISE J175510.28+180320.2	T1.0	16.02±0.09	16.02±0.09	2	39.00	27;1; ...
2MASS J21171431–2940034	T0.0	15.601±0.06	14.15±0.07	2	21.40	3;3; ...
2MASS J21392676+0220226	T2.0	15.264±0.05	13.582±0.04	2	10.00	5;9; ...
2MASS J22092183–2711329	T2.0	>15.786	>15.097	2	45.00	38;1; ...
2MASS J22120703+3430351	L7.0	16.316±0.1	14.37±0.07	2	11.00	9;1; ...
ULAS J222958.30+010217.2	T3.0	17.88±0.02	...	6	11.00	38;17; ...
WISEA J223343.53–133140.9	T2.0	16.451±0.13	15.494±0.22	2	19.60	36;1; ...
WISE J223937.55+161716.1	T3.0	16.079±0.08	>14.89	6	50.00	20;1; ...
WISE J232728.74–273056.6	T0.0	16.681±0.14	14.756±0.1	2	41.00	20;1; ...
2MASS J23322678+1234530	T0.0	16.89±0.19	15.7±0.31	2	29.80	21;21; ...

Table A.2 *continued on next page*

Table A.2 (*continued*)

Source	SpeX SpT	<i>J</i> mag	<i>K</i> mag	Total	SNR	Reference ^a
--------	----------	--------------	--------------	-------	-----	------------------------

References—(1) This paper; (2) Best et al. (2013); (3) Best et al. (2015); (4) Burgasser et al. (2004); (5) Burgasser et al. (2006a); (6) Burgasser et al. (2006b); (7) Burgasser (2007b); (8) Burgasser et al. (2008); (9) Burgasser et al. (2010); (10) Burgasser et al. (2013); (11) Bardalez Gagliuffi et al. (2015); (12) Chiu et al. (2006); (13) Cruz et al. (2004); (14) Deacon et al. (2011); (15) Dupuy & Liu (2012); (16) Deacon et al. (2012); (17) Day-Jones et al. (2013); (18) Gelino et al. (2014); (19) Geifler et al. (2011); (20) Kirkpatrick et al. (2011); (21) Kellogg et al. (2015); (22) Kellogg et al. (2017) (23) Luhman (2013); (24) Looper et al. (2007); (25) Liu et al. (2010); (26) Luhman et al. (2007); (27) Luhman & Sheppard (2014); (28) Liu et al. (2006); (29) Mace et al. (2013); (30) Manjavacas et al. (2013); (31) Metchev et al. (2008); (32) Robert et al. (2016); (33) Reid et al. (2006b); (34) Sheppard & Cushing (2009); (35) Schneider et al. (2017); (36) Schneider et al. (2016a); (37) Thompson et al. (2013); (38) Burgasser et al. inprep.

^aSpectrum; Spectral Binary Candidate; Confirmed Binarity/Variability

REFERENCES

- Ackerman, A. S., & Marley, M. S. 2001, *ApJ*, 556, 872, doi: [10.1086/321540](https://doi.org/10.1086/321540)
- Allers, K. N., & Liu, M. C. 2013, *ApJ*, 772, 79, doi: [10.1088/0004-637X/772/2/79](https://doi.org/10.1088/0004-637X/772/2/79)
- Apai, D., Nardiello, D., & Bedin, L. R. 2021, *ApJ*, 906, 64, doi: [10.3847/1538-4357/abcb97](https://doi.org/10.3847/1538-4357/abcb97)
- Apai, D., Radigan, J., Buenzli, E., et al. 2013, *ApJ*, 768, 121, doi: [10.1088/0004-637X/768/2/121](https://doi.org/10.1088/0004-637X/768/2/121)
- Apai, D., Kasper, M., Skemer, A., et al. 2016, *ApJ*, 820, 40, doi: [10.3847/0004-637X/820/1/40](https://doi.org/10.3847/0004-637X/820/1/40)
- Apai, D., Karalidi, T., Marley, M. S., et al. 2017, *Science*, 357, 683, doi: [10.1126/science.aam9848](https://doi.org/10.1126/science.aam9848)
- Bardalez Gagliuffi, D. C., Gelino, C. R., & Burgasser, A. J. 2015, *AJ*, 150, 163, doi: [10.1088/0004-6256/150/5/163](https://doi.org/10.1088/0004-6256/150/5/163)
- Bardalez Gagliuffi, D. C., Burgasser, A. J., Gelino, C. R., et al. 2014, *ApJ*, 794, 143, doi: [10.1088/0004-637X/794/2/143](https://doi.org/10.1088/0004-637X/794/2/143)
- Bardalez Gagliuffi, D. C., Burgasser, A. J., Schmidt, S. J., et al. 2019, *ApJ*, 883, 205, doi: [10.3847/1538-4357/ab253d](https://doi.org/10.3847/1538-4357/ab253d)
- Barrado y Navascués, D., Stauffer, J. R., & Jayawardhana, R. 2004, *ApJ*, 614, 386, doi: [10.1086/423485](https://doi.org/10.1086/423485)
- Best, W. M. J., Liu, M. C., Magnier, E. A., & Dupuy, T. J. 2020, *AJ*, 159, 257, doi: [10.3847/1538-3881/ab84f4](https://doi.org/10.3847/1538-3881/ab84f4)
- . 2021, *AJ*, 161, 42, doi: [10.3847/1538-3881/abc893](https://doi.org/10.3847/1538-3881/abc893)
- Best, W. M. J., Liu, M. C., Magnier, E. A., et al. 2013, *ApJ*, 777, 84, doi: [10.1088/0004-637X/777/2/84](https://doi.org/10.1088/0004-637X/777/2/84)
- Best, W. M. J., Liu, M. C., Magnier, E. A., et al. 2015, *ApJ*, 814, 118, doi: [10.1088/0004-637X/814/2/118](https://doi.org/10.1088/0004-637X/814/2/118)
- Best, W. M. J., Liu, M. C., Magnier, E. A., et al. 2017, *ApJ*, 837, 95, doi: [10.3847/1538-4357/aa5df0](https://doi.org/10.3847/1538-4357/aa5df0)
- Biller, B. A., Crossfield, I. J. M., Mancini, L., et al. 2013, *ApJL*, 778, L10, doi: [10.1088/2041-8205/778/1/L10](https://doi.org/10.1088/2041-8205/778/1/L10)
- Biller, B. A., Apai, D., Bonnefoy, M., et al. 2021, *MNRAS*, 503, 743, doi: [10.1093/mnras/stab202](https://doi.org/10.1093/mnras/stab202)
- Booth, M., del Burgo, C., & Hambaryan, V. V. 2021, *MNRAS*, 500, 5552, doi: [10.1093/mnras/staa3631](https://doi.org/10.1093/mnras/staa3631)
- Bouy, H., Brandner, W., Martín, E. L., et al. 2003, *AJ*, 126, 1526, doi: [10.1086/377343](https://doi.org/10.1086/377343)
- Brandt, T. D., & Huang, C. X. 2015, *ApJ*, 807, 58, doi: [10.1088/0004-637X/807/1/58](https://doi.org/10.1088/0004-637X/807/1/58)
- Brock, L., Barman, T., Konopacky, Q. M., & Stone, J. M. 2021, *ApJ*, 914, 124, doi: [10.3847/1538-4357/abfc46](https://doi.org/10.3847/1538-4357/abfc46)

- Buenzli, E., Apai, D., Radigan, J., Reid, I. N., & Flateau, D. 2014, *ApJ*, 782, 77, doi: [10.1088/0004-637X/782/2/77](https://doi.org/10.1088/0004-637X/782/2/77)
- Buenzli, E., Marley, M. S., Apai, D., et al. 2015a, *ApJ*, 812, 163, doi: [10.1088/0004-637X/812/2/163](https://doi.org/10.1088/0004-637X/812/2/163)
- Buenzli, E., Saumon, D., Marley, M. S., et al. 2015b, *ApJ*, 798, 127, doi: [10.1088/0004-637X/798/2/127](https://doi.org/10.1088/0004-637X/798/2/127)
- Burgasser, A. J. 2007a, *ApJ*, 659, 655, doi: [10.1086/511027](https://doi.org/10.1086/511027)
- . 2007b, *AJ*, 134, 1330, doi: [10.1086/520878](https://doi.org/10.1086/520878)
- Burgasser, A. J. 2014, in *Astronomical Society of India Conference Series*, Vol. 11, *Astronomical Society of India Conference Series*, 7–16. <https://arxiv.org/abs/1406.4887>
- Burgasser, A. J., Bardalez-Gagliuffi, D. C., & Gizis, J. E. 2011, *AJ*, 141, 70, doi: [10.1088/0004-6256/141/3/70](https://doi.org/10.1088/0004-6256/141/3/70)
- Burgasser, A. J., Blake, C. H., Gelino, C. R., Sahlmann, J., & Bardalez Gagliuffi, D. 2016, *ApJ*, 827, 25, doi: [10.3847/0004-637X/827/1/25](https://doi.org/10.3847/0004-637X/827/1/25)
- Burgasser, A. J., Cruz, K. L., Cushing, M., et al. 2010, *ApJ*, 710, 1142, doi: [10.1088/0004-637X/710/2/1142](https://doi.org/10.1088/0004-637X/710/2/1142)
- Burgasser, A. J., Geballe, T. R., Leggett, S. K., Kirkpatrick, J. D., & Golimowski, D. A. 2006a, *ApJ*, 637, 1067, doi: [10.1086/498563](https://doi.org/10.1086/498563)
- Burgasser, A. J., Kirkpatrick, J. D., Cruz, K. L., et al. 2006b, *ApJS*, 166, 585, doi: [10.1086/506327](https://doi.org/10.1086/506327)
- Burgasser, A. J., Kirkpatrick, J. D., Liebert, J., & Burrows, A. 2003, *ApJ*, 594, 510, doi: [10.1086/376756](https://doi.org/10.1086/376756)
- Burgasser, A. J., Liu, M. C., Ireland, M. J., Cruz, K. L., & Dupuy, T. J. 2008, *ApJ*, 681, 579, doi: [10.1086/588379](https://doi.org/10.1086/588379)
- Burgasser, A. J., Marley, M. S., Ackerman, A. S., et al. 2002a, *ApJL*, 571, L151, doi: [10.1086/341343](https://doi.org/10.1086/341343)
- Burgasser, A. J., McElwain, M. W., Kirkpatrick, J. D., et al. 2004, *AJ*, 127, 2856, doi: [10.1086/383549](https://doi.org/10.1086/383549)
- Burgasser, A. J., Reid, I. N., Leggett, S. K., et al. 2005, *ApJL*, 634, L177, doi: [10.1086/498866](https://doi.org/10.1086/498866)
- Burgasser, A. J., Sheppard, S. S., & Luhman, K. L. 2013, *ApJ*, 772, 129, doi: [10.1088/0004-637X/772/2/129](https://doi.org/10.1088/0004-637X/772/2/129)
- Burgasser, A. J., & Splat Development Team. 2017, in *Astronomical Society of India Conference Series*, Vol. 14, *Astronomical Society of India Conference Series*, 7–12. <https://arxiv.org/abs/1707.00062>
- Burgasser, A. J., Kirkpatrick, J. D., Brown, M. E., et al. 1999, *ApJL*, 522, L65, doi: [10.1086/312221](https://doi.org/10.1086/312221)
- Burgasser, A. J., Kirkpatrick, J. D., Cutri, R. M., et al. 2000, *ApJL*, 531, L57, doi: [10.1086/312522](https://doi.org/10.1086/312522)
- Burgasser, A. J., Kirkpatrick, J. D., Brown, M. E., et al. 2002b, *ApJ*, 564, 421, doi: [10.1086/324033](https://doi.org/10.1086/324033)
- Carter, A. L., Hinkley, S., Bonavita, M., et al. 2021, *MNRAS*, 501, 1999, doi: [10.1093/mnras/staa3579](https://doi.org/10.1093/mnras/staa3579)
- Chiu, K., Fan, X., Leggett, S. K., et al. 2006, *AJ*, 131, 2722, doi: [10.1086/501431](https://doi.org/10.1086/501431)
- Cruz, K. L., Burgasser, A. J., Reid, I. N., & Liebert, J. 2004, *ApJL*, 604, L61, doi: [10.1086/383415](https://doi.org/10.1086/383415)
- Cruz, K. L., Reid, I. N., Kirkpatrick, J. D., et al. 2007, *AJ*, 133, 439, doi: [10.1086/510132](https://doi.org/10.1086/510132)
- Dahn, C. C., Harris, H. C., Vrba, F. J., et al. 2002, *AJ*, 124, 1170, doi: [10.1086/341646](https://doi.org/10.1086/341646)
- Day-Jones, A. C., Marocco, F., Pinfield, D. J., et al. 2013, *MNRAS*, 648, doi: [10.1093/mnras/sts685](https://doi.org/10.1093/mnras/sts685)
- Deacon, N. R., Liu, M. C., Magnier, E. A., et al. 2011, *AJ*, 142, 77, doi: [10.1088/0004-6256/142/3/77](https://doi.org/10.1088/0004-6256/142/3/77)
- . 2012, *ApJ*, 757, 100, doi: [10.1088/0004-637X/757/1/100](https://doi.org/10.1088/0004-637X/757/1/100)
- Dupuy, T. J., & Liu, M. C. 2012, *ApJS*, 201, 19, doi: [10.1088/0067-0049/201/2/19](https://doi.org/10.1088/0067-0049/201/2/19)
- Enoch, M. L., Brown, M. E., & Burgasser, A. J. 2003, *AJ*, 126, 1006, doi: [10.1086/376598](https://doi.org/10.1086/376598)

- Eriksson, S. C., Janson, M., & Calissendorff, P. 2019, *A&A*, 629, A145, doi: [10.1051/0004-6361/201935671](https://doi.org/10.1051/0004-6361/201935671)
- Faherty, J. K., Beletsky, Y., Burgasser, A. J., et al. 2014, *ApJ*, 790, 90, doi: [10.1088/0004-637X/790/2/90](https://doi.org/10.1088/0004-637X/790/2/90)
- Faherty, J. K., Burgasser, A. J., Bochanski, J. J., et al. 2011, *AJ*, 141, 71, doi: [10.1088/0004-6256/141/3/71](https://doi.org/10.1088/0004-6256/141/3/71)
- Faherty, J. K., Burgasser, A. J., Cruz, K. L., et al. 2009, *AJ*, 137, 1, doi: [10.1088/0004-6256/137/1/1](https://doi.org/10.1088/0004-6256/137/1/1)
- Faherty, J. K., Riedel, A. R., Cruz, K. L., et al. 2016, *ApJS*, 225, 10, doi: [10.3847/0067-0049/225/1/10](https://doi.org/10.3847/0067-0049/225/1/10)
- Filippazzo, J. C., Rice, E. L., Faherty, J., et al. 2015, *ApJ*, 810, 158, doi: [10.1088/0004-637X/810/2/158](https://doi.org/10.1088/0004-637X/810/2/158)
- Gagné, J., Allers, K. N., Theissen, C. A., et al. 2018a, *ApJL*, 854, L27, doi: [10.3847/2041-8213/aaacfd](https://doi.org/10.3847/2041-8213/aaacfd)
- Gagné, J., Lafrenière, D., Doyon, R., Malo, L., & Artigau, É. 2014, *ApJ*, 783, 121, doi: [10.1088/0004-637X/783/2/121](https://doi.org/10.1088/0004-637X/783/2/121)
- Gagné, J., Lafrenière, D., Doyon, R., Malo, L., & Artigau, É. 2015a, *The Astrophysical Journal*, 798, 73, doi: [10.1088/0004-637X/798/2/73](https://doi.org/10.1088/0004-637X/798/2/73)
- Gagné, J., Faherty, J. K., Cruz, K. L., et al. 2015b, *The Astrophysical Journal Supplement Series*, 219, 33, doi: [10.1088/0067-0049/219/2/33](https://doi.org/10.1088/0067-0049/219/2/33)
- Gagné, J., Faherty, J. K., Burgasser, A. J., et al. 2017a, *ApJL*, 841, L1, doi: [10.3847/2041-8213/aa70e2](https://doi.org/10.3847/2041-8213/aa70e2)
- Gagné, J., Faherty, J. K., Mamajek, E. E., et al. 2017b, *ApJS*, 228, 18, doi: [10.3847/1538-4365/228/2/18](https://doi.org/10.3847/1538-4365/228/2/18)
- Gagné, J., Mamajek, E. E., Malo, L., et al. 2018b, *ApJ*, 856, 23, doi: [10.3847/1538-4357/aaae09](https://doi.org/10.3847/1538-4357/aaae09)
- Gauza, B., Béjar, V. J. S., Pérez-Garrido, A., et al. 2019, *MNRAS*, 487, 1149, doi: [10.1093/mnras/stz1284](https://doi.org/10.1093/mnras/stz1284)
- Ge, H., Zhang, X., Fletcher, L. N., et al. 2019, *AJ*, 157, 89, doi: [10.3847/1538-3881/aafba7](https://doi.org/10.3847/1538-3881/aafba7)
- Geballe, T. R., Knapp, G. R., Leggett, S. K., et al. 2002, *ApJ*, 564, 466, doi: [10.1086/324078](https://doi.org/10.1086/324078)
- Geißler, K., Metchev, S., Kirkpatrick, J. D., Berriman, G. B., &Looper, D. 2011, *ApJ*, 732, 56, doi: [10.1088/0004-637X/732/1/56](https://doi.org/10.1088/0004-637X/732/1/56)
- Gelino, C. R., Marley, M. S., Holtzman, J. A., Ackerman, A. S., & Lodders, K. 2002, *ApJ*, 577, 433, doi: [10.1086/342150](https://doi.org/10.1086/342150)
- Gelino, C. R., Smart, R. L., Marocco, F., et al. 2014, *AJ*, 148, 6, doi: [10.1088/0004-6256/148/1/6](https://doi.org/10.1088/0004-6256/148/1/6)
- Gillon, M., Triaud, A. H. M. J., Jehin, E., et al. 2013, *A&A*, 555, L5, doi: [10.1051/0004-6361/201321620](https://doi.org/10.1051/0004-6361/201321620)
- Girardin, F., Artigau, É., & Doyon, R. 2013, *ApJ*, 767, 61, doi: [10.1088/0004-637X/767/1/61](https://doi.org/10.1088/0004-637X/767/1/61)
- Gizis, J. E. 2002, *ApJ*, 575, 484, doi: [10.1086/341259](https://doi.org/10.1086/341259)
- Gizis, J. E., Allers, K. N., Liu, M. C., et al. 2015, *ApJ*, 799, 203, doi: [10.1088/0004-637X/799/2/203](https://doi.org/10.1088/0004-637X/799/2/203)
- Gizis, J. E., Faherty, J. K., Liu, M. C., et al. 2012, *AJ*, 144, 94, doi: [10.1088/0004-6256/144/4/94](https://doi.org/10.1088/0004-6256/144/4/94)
- Hawley, S. L. 1993, *PASP*, 105, 955, doi: [10.1086/133262](https://doi.org/10.1086/133262)
- Hawley, S. L., Covey, K. R., Knapp, G. R., et al. 2002, *AJ*, 123, 3409, doi: [10.1086/340697](https://doi.org/10.1086/340697)
- Henry, T. J., Jao, W.-C., Winters, J. G., et al. 2018, *AJ*, 155, 265, doi: [10.3847/1538-3881/aac262](https://doi.org/10.3847/1538-3881/aac262)
- Jackson, R. J., & Jeffries, R. D. 2010, *MNRAS*, 402, 1380, doi: [10.1111/j.1365-2966.2009.15983.x](https://doi.org/10.1111/j.1365-2966.2009.15983.x)
- Kaiser, N., Burgett, W., Chambers, K., et al. 2010, in *Society of Photo-Optical Instrumentation Engineers (SPIE) Conference Series*, Vol. 7733, *Ground-based and Airborne Telescopes III*, ed. L. M. Stepp, R. Gilmozzi, & H. J. Hall, 77330E, doi: [10.1117/12.859188](https://doi.org/10.1117/12.859188)
- Kao, M. M., Hallinan, G., Pineda, J. S., Stevenson, D., & Burgasser, A. 2018, *ApJS*, 237, 25, doi: [10.3847/1538-4365/aac2d5](https://doi.org/10.3847/1538-4365/aac2d5)

- Kellogg, K., Metchev, S., Geißler, K., et al. 2015, *AJ*, 150, 182, doi: [10.1088/0004-6256/150/6/182](https://doi.org/10.1088/0004-6256/150/6/182)
- Kellogg, K., Metchev, S., Miles-Páez, P. A., & Tannock, M. E. 2017, *AJ*, 154, 112, doi: [10.3847/1538-3881/aa83b0](https://doi.org/10.3847/1538-3881/aa83b0)
- Khandrika, H., Burgasser, A. J., Melis, C., et al. 2013, *AJ*, 145, 71, doi: [10.1088/0004-6256/145/3/71](https://doi.org/10.1088/0004-6256/145/3/71)
- Kirkpatrick, J. D., Reid, I. N., Liebert, J., et al. 2000, *AJ*, 120, 447, doi: [10.1086/301427](https://doi.org/10.1086/301427)
- Kirkpatrick, J. D., Cruz, K. L., Barman, T. S., et al. 2008, *ApJ*, 689, 1295, doi: [10.1086/592768](https://doi.org/10.1086/592768)
- Kirkpatrick, J. D., Looper, D. L., Burgasser, A. J., et al. 2010, *ApJS*, 190, 100, doi: [10.1088/0067-0049/190/1/100](https://doi.org/10.1088/0067-0049/190/1/100)
- Kirkpatrick, J. D., Cushing, M. C., Gelino, C. R., et al. 2011, *ApJS*, 197, 19, doi: [10.1088/0067-0049/197/2/19](https://doi.org/10.1088/0067-0049/197/2/19)
- Kirkpatrick, J. D., Gelino, C. R., Faherty, J. K., et al. 2021, *ApJS*, 253, 7, doi: [10.3847/1538-4365/abd107](https://doi.org/10.3847/1538-4365/abd107)
- Knapp, G. R., Leggett, S. K., Fan, X., et al. 2004, *AJ*, 127, 3553, doi: [10.1086/420707](https://doi.org/10.1086/420707)
- Kniazev, A. Y., Vaisanen, P., Mužić, K., et al. 2013, *ApJ*, 770, 124, doi: [10.1088/0004-637X/770/2/124](https://doi.org/10.1088/0004-637X/770/2/124)
- Koen, C. 2005, *MNRAS*, 360, 1132, doi: [10.1111/j.1365-2966.2005.09119.x](https://doi.org/10.1111/j.1365-2966.2005.09119.x)
- Koen, C., Tanabé, T., Tamura, M., & Kusakabe, N. 2005, *MNRAS*, 362, 727, doi: [10.1111/j.1365-2966.2005.09280.x](https://doi.org/10.1111/j.1365-2966.2005.09280.x)
- Lew, B. W. P., Apai, D., Zhou, Y., et al. 2016, *ApJL*, 829, L32, doi: [10.3847/2041-8205/829/2/L32](https://doi.org/10.3847/2041-8205/829/2/L32)
- Lindegren, L., Klioner, S. A., Hernández, J., et al. 2021, *A&A*, 649, A2, doi: [10.1051/0004-6361/202039709](https://doi.org/10.1051/0004-6361/202039709)
- Liu, M. C., Dupuy, T. J., & Allers, K. N. 2016, *ApJ*, 833, 96, doi: [10.3847/1538-4357/833/1/96](https://doi.org/10.3847/1538-4357/833/1/96)
- Liu, M. C., Dupuy, T. J., & Leggett, S. K. 2010, *ApJ*, 722, 311, doi: [10.1088/0004-637X/722/1/311](https://doi.org/10.1088/0004-637X/722/1/311)
- Liu, M. C., Leggett, S. K., Golimowski, D. A., et al. 2006, *ApJ*, 647, 1393, doi: [10.1086/505561](https://doi.org/10.1086/505561)
- Liu, M. C., Magnier, E. A., Deacon, N. R., et al. 2013, *ApJL*, 777, L20, doi: [10.1088/2041-8205/777/2/L20](https://doi.org/10.1088/2041-8205/777/2/L20)
- Lodders, K., & Fegley, Jr., B. 2006, *Chemistry of Low Mass Substellar Objects* (Springer Praxis Books), 1, doi: [10.1007/3-540-30313-8_1](https://doi.org/10.1007/3-540-30313-8_1)
- Looper, D. L., Kirkpatrick, J. D., & Burgasser, A. J. 2007, *AJ*, 134, 1162, doi: [10.1086/520645](https://doi.org/10.1086/520645)
- Looper, D. L., Kirkpatrick, J. D., Cutri, R. M., et al. 2008, *ApJ*, 686, 528, doi: [10.1086/591025](https://doi.org/10.1086/591025)
- Luger, R., Agol, E., Foreman-Mackey, D., et al. 2019, *AJ*, 157, 64, doi: [10.3847/1538-3881/aae8e5](https://doi.org/10.3847/1538-3881/aae8e5)
- Luhman, K. L. 2013, *ApJL*, 767, L1, doi: [10.1088/2041-8205/767/1/L1](https://doi.org/10.1088/2041-8205/767/1/L1)
- Luhman, K. L., & Sheppard, S. S. 2014, *ApJ*, 787, 126, doi: [10.1088/0004-637X/787/2/126](https://doi.org/10.1088/0004-637X/787/2/126)
- Luhman, K. L., Patten, B. M., Marengo, M., et al. 2007, *ApJ*, 654, 570, doi: [10.1086/509073](https://doi.org/10.1086/509073)
- Mace, G. N., Kirkpatrick, J. D., Cushing, M. C., et al. 2013, *ApJS*, 205, 6, doi: [10.1088/0067-0049/205/1/6](https://doi.org/10.1088/0067-0049/205/1/6)
- Madhusudhan, N., Knutson, H., Fortney, J. J., & Barman, T. 2014, in *Protostars and Planets VI*, ed. H. Beuther, R. S. Klessen, C. P. Dullemond, & T. Henning, 739, doi: [10.2458/azu_uapress_9780816531240-ch032](https://doi.org/10.2458/azu_uapress_9780816531240-ch032)
- Manjavacas, E., Goldman, B., Reffert, S., & Henning, T. 2013, *A&A*, 560, A52, doi: [10.1051/0004-6361/201321720](https://doi.org/10.1051/0004-6361/201321720)
- Manjavacas, E., Goldman, B., Alcalá, J. M., et al. 2016, *MNRAS*, 455, 1341, doi: [10.1093/mnras/stv2048](https://doi.org/10.1093/mnras/stv2048)
- Manjavacas, E., Apai, D., Zhou, Y., et al. 2019, *AJ*, 157, 101, doi: [10.3847/1538-3881/aaf88f](https://doi.org/10.3847/1538-3881/aaf88f)
- Marley, M. S., Saumon, D., Cushing, M., et al. 2012, *ApJ*, 754, 135, doi: [10.1088/0004-637X/754/2/135](https://doi.org/10.1088/0004-637X/754/2/135)
- Metchev, S. A., Kirkpatrick, J. D., Berriman, G. B., & Looper, D. 2008, *ApJ*, 676, 1281, doi: [10.1086/524721](https://doi.org/10.1086/524721)

- Metchev, S. A., Heinze, A., Apai, D., et al. 2015, *ApJ*, 799, 154, doi: [10.1088/0004-637X/799/2/154](https://doi.org/10.1088/0004-637X/799/2/154)
- Millar-Blanchaer, M. A., Girard, J. H., Karalidi, T., et al. 2020, *ApJ*, 894, 42, doi: [10.3847/1538-4357/ab6ef2](https://doi.org/10.3847/1538-4357/ab6ef2)
- Morales-Calderón, M., Stauffer, J. R., Kirkpatrick, J. D., et al. 2006, *ApJ*, 653, 1454, doi: [10.1086/507866](https://doi.org/10.1086/507866)
- Ochsenbein, F., Bauer, P., & Marcout, J. 2000, *A&AS*, 143, 23, doi: [10.1051/aas:2000169](https://doi.org/10.1051/aas:2000169)
- Pineda, J. S., Hallinan, G., Kirkpatrick, J. D., et al. 2016, *ApJ*, 826, 73, doi: [10.3847/0004-637X/826/1/73](https://doi.org/10.3847/0004-637X/826/1/73)
- Radigan, J. 2014, *ApJ*, 797, 120, doi: [10.1088/0004-637X/797/2/120](https://doi.org/10.1088/0004-637X/797/2/120)
- Radigan, J., Jayawardhana, R., Lafrenière, D., et al. 2012, *ApJ*, 750, 105, doi: [10.1088/0004-637X/750/2/105](https://doi.org/10.1088/0004-637X/750/2/105)
- Radigan, J., Lafrenière, D., Jayawardhana, R., & Artigau, E. 2014, *ApJ*, 793, 75, doi: [10.1088/0004-637X/793/2/75](https://doi.org/10.1088/0004-637X/793/2/75)
- Rayner, J. T., Toomey, D. W., Onaka, P. M., et al. 2003, *PASP*, 115, 362, doi: [10.1086/367745](https://doi.org/10.1086/367745)
- Reid, I. N., Cruz, K. L., Kirkpatrick, J. D., et al. 2008, *AJ*, 136, 1290, doi: [10.1088/0004-6256/136/3/1290](https://doi.org/10.1088/0004-6256/136/3/1290)
- Reid, I. N., Lewitus, E., Allen, P. R., Cruz, K. L., & Burgasser, A. J. 2006a, *AJ*, 132, 891, doi: [10.1086/505626](https://doi.org/10.1086/505626)
- Reid, I. N., Lewitus, E., Burgasser, A. J., & Cruz, K. L. 2006b, *ApJ*, 639, 1114, doi: [10.1086/499484](https://doi.org/10.1086/499484)
- Reid, I. N., Kirkpatrick, J. D., Liebert, J., et al. 1999, *ApJ*, 521, 613, doi: [10.1086/307589](https://doi.org/10.1086/307589)
- Robert, J., Gagné, J., Artigau, É., et al. 2016, *ApJ*, 830, 144, doi: [10.3847/0004-637X/830/2/144](https://doi.org/10.3847/0004-637X/830/2/144)
- Sahlmann, J., Burgasser, A. J., Bardalez Gagliuffi, D. C., et al. 2020, *MNRAS*, 495, 1136, doi: [10.1093/mnras/staa1235](https://doi.org/10.1093/mnras/staa1235)
- Schmidt, S. J., Cruz, K. L., Bongiorno, B. J., Liebert, J., & Reid, I. N. 2007, *AJ*, 133, 2258, doi: [10.1086/512158](https://doi.org/10.1086/512158)
- Schneider, A. C., Cushing, M. C., Kirkpatrick, J. D., et al. 2014, *AJ*, 147, 34, doi: [10.1088/0004-6256/147/2/34](https://doi.org/10.1088/0004-6256/147/2/34)
- Schneider, A. C., Greco, J., Cushing, M. C., et al. 2016a, *ApJ*, 817, 112, doi: [10.3847/0004-637X/817/2/112](https://doi.org/10.3847/0004-637X/817/2/112)
- Schneider, A. C., Hardegree-Ullman, K. K., Cushing, M. C., Kirkpatrick, J. D., & Shkolnik, E. L. 2018, *AJ*, 155, 238, doi: [10.3847/1538-3881/aabfc2](https://doi.org/10.3847/1538-3881/aabfc2)
- Schneider, A. C., Windsor, J., Cushing, M. C., Kirkpatrick, J. D., & Shkolnik, E. L. 2017, *AJ*, 153, 196, doi: [10.3847/1538-3881/aa6624](https://doi.org/10.3847/1538-3881/aa6624)
- Schneider, A. C., Windsor, J., Cushing, M. C., Kirkpatrick, J. D., & Wright, E. L. 2016b, *ApJL*, 822, L1, doi: [10.3847/2041-8205/822/1/L1](https://doi.org/10.3847/2041-8205/822/1/L1)
- Scholz, R.-D. 2010, *A&A*, 510, L8, doi: [10.1051/0004-6361/201014078](https://doi.org/10.1051/0004-6361/201014078)
- Sheppard, S. S., & Cushing, M. C. 2009, *AJ*, 137, 304, doi: [10.1088/0004-6256/137/1/304](https://doi.org/10.1088/0004-6256/137/1/304)
- Showman, A. P., Tan, X., & Zhang, X. 2019, *ApJ*, 883, 4, doi: [10.3847/1538-4357/ab384a](https://doi.org/10.3847/1538-4357/ab384a)
- Song, I., Zuckerman, B., & Bessell, M. S. 2012, *AJ*, 144, 8, doi: [10.1088/0004-6256/144/1/8](https://doi.org/10.1088/0004-6256/144/1/8)
- Tan, X., & Showman, A. P. 2021a, *MNRAS*, 502, 2198, doi: [10.1093/mnras/stab097](https://doi.org/10.1093/mnras/stab097)
- . 2021b, *MNRAS*, 502, 678, doi: [10.1093/mnras/stab060](https://doi.org/10.1093/mnras/stab060)
- Thompson, M. A., Kirkpatrick, J. D., Mace, G. N., et al. 2013, *PASP*, 125, 809, doi: [10.1086/671426](https://doi.org/10.1086/671426)
- Tinney, C. G., Burgasser, A. J., & Kirkpatrick, J. D. 2003, *AJ*, 126, 975, doi: [10.1086/376481](https://doi.org/10.1086/376481)
- Tremblin, P., Amundsen, D. S., Chabrier, G., et al. 2016, *ApJL*, 817, L19, doi: [10.3847/2041-8205/817/2/L19](https://doi.org/10.3847/2041-8205/817/2/L19)
- Tremblin, P., Amundsen, D. S., Mourier, P., et al. 2015, *ApJL*, 804, L17, doi: [10.1088/2041-8205/804/1/L17](https://doi.org/10.1088/2041-8205/804/1/L17)
- Tremblin, P., Phillips, M. W., Emery, A., et al. 2020, *A&A*, 643, A23, doi: [10.1051/0004-6361/202038771](https://doi.org/10.1051/0004-6361/202038771)

- Tremblin, P., Chabrier, G., Baraffe, I., et al. 2017, *ApJ*, 850, 46,
doi: [10.3847/1538-4357/aa9214](https://doi.org/10.3847/1538-4357/aa9214)
- Tremblin, P., Padioleau, T., Phillips, M. W., et al. 2019, *ApJ*, 876, 144,
doi: [10.3847/1538-4357/ab05db](https://doi.org/10.3847/1538-4357/ab05db)
- Vacca, W. D., Cushing, M. C., & Rayner, J. T. 2003, *PASP*, 115, 389,
doi: [10.1086/346193](https://doi.org/10.1086/346193)
- Vos, J., Allers, K., Apai, D., et al. 2019a, *BAAS*, 51, 253
- Vos, J. M., Allers, K. N., & Biller, B. A. 2017, *ApJ*, 842, 78,
doi: [10.3847/1538-4357/aa73cf](https://doi.org/10.3847/1538-4357/aa73cf)
- Vos, J. M., Allers, K. N., Biller, B. A., et al. 2018, *MNRAS*, 474, 1041,
doi: [10.1093/mnras/stx2752](https://doi.org/10.1093/mnras/stx2752)
- Vos, J. M., Faherty, J. K., Gagné, J., et al. 2022, *ApJ*, 924, 68,
doi: [10.3847/1538-4357/ac4502](https://doi.org/10.3847/1538-4357/ac4502)
- Vos, J. M., Biller, B. A., Bonavita, M., et al. 2019b, *MNRAS*, 483, 480,
doi: [10.1093/mnras/sty3123](https://doi.org/10.1093/mnras/sty3123)
- Vos, J. M., Biller, B. A., Allers, K. N., et al. 2020, *AJ*, 160, 38,
doi: [10.3847/1538-3881/ab9642](https://doi.org/10.3847/1538-3881/ab9642)
- Vrba, F. J., Henden, A. A., Luginbuhl, C. B., et al. 2004, *AJ*, 127, 2948,
doi: [10.1086/383554](https://doi.org/10.1086/383554)
- Wenger, M., Ochsenbein, F., Egret, D., et al. 2000, *A&AS*, 143, 9,
doi: [10.1051/aas:2000332](https://doi.org/10.1051/aas:2000332)
- Wright, E. L., Eisenhardt, P. R. M., Mainzer, A. K., et al. 2010, *AJ*, 140, 1868,
doi: [10.1088/0004-6256/140/6/1868](https://doi.org/10.1088/0004-6256/140/6/1868)
- Zhang, Z., Liu, M. C., Best, W. M. J., Dupuy, T. J., & Siverd, R. J. 2021, *ApJ*, 911, 7,
doi: [10.3847/1538-4357/abe3fa](https://doi.org/10.3847/1538-4357/abe3fa)
- Zuckerman, B. 2019, *ApJ*, 870, 27,
doi: [10.3847/1538-4357/aace66](https://doi.org/10.3847/1538-4357/aace66)